Microstructure Development in DMLS IN718

By

Blake Rogers

Thesis Defense

Committee Members:

Amaneh Tasooji(Chair)
William Petuskey
Brad Rogers

Abstract

DMLS processed IN718 was studied to identify possible microstructural differences that could lead to an improved creep resistance over conventionally wrought IN718.

Creep rupture curves for both types of sample were used to calculate steady-state creep rates. These rates were used to create a creep model based on power-law and Sinh creep laws.

SEM and TEM studies showed a increased number of precipitates in DMLS IN718 and especially along grain boundaries.

Thermal modeling and literature suggest that high cooling rates can lead to high residual stresses that encourage preferred strengthening phases.

Presentation Layout

- Problem Statement
- Approach
- Introduction
- Microstructure and Properties of IN718
- Analysis of Creep Data
- SEM Study
- TEM Sample Prep
- TEM Study
- Thermal Modeling
- Summary and Conclusion

Problem Statement

Inconel alloy 718 showed an increased resistance to creep

Limited information regarding this phenomenon was available

Reasons for this increased resistance were theorized and investigated using available resources

Approach

A literature review of DMLS processing and IN718 was performed to identify possible creep inhibitors

Creep rupture data was used to model the creep mechanisms active in DMLS and wrought IN718

SEM and TEM studies were used to confirm findings from literature review and creep study, and to identify other possible mechanisms

Thermal modeling was used to identify complex microstructural development of DMLS processed materials

Nickel Alloys are Introduced and Help Revolutionize Aerospace

- Monel alloy 400 (1906)
  - Ambrose Monell
- Inconel alloy X-750 (1940's)
  - X-15 rocket-powered hypersonic vehicle
- Inconel alloy 718 (1960's)
  - Developed as result of γ', γ'' discovery during 625 aging tests
- Inconel alloy 625 (1960's)
  - H. L. Eiselstein

Inconel 718, The Favored Nickel Alloy for the Past Half Century

- Most popular nickel alloy used today
- Many uses from rocket nozzles to turbine discs and cryogenic tankage
- Precipitate strengthened
- Creep resistant
- Good weldability
- Corrosion resistant

Additive Manufacturing & Direct Metal Laser Sintering (DMLS) Processing Used in Manufacturing Aerospace Components

- Developed by EOS (1990's)
- Utilizes atomized metal powders
- Laser scans surface of powder to fuse layers
- Melting and cooling rates very high
- Solidification leads to high residual stress

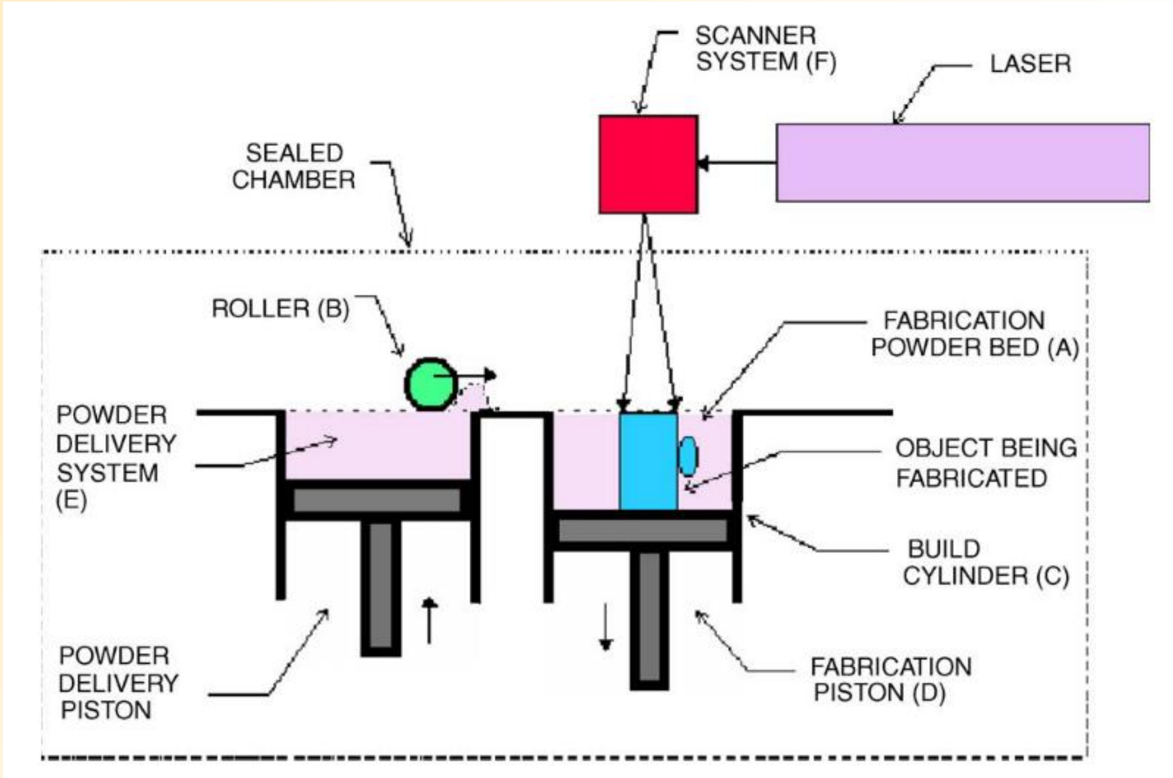

Illustration of selective laser sintering process. Source: E.C. Santos, M. Shiomi, K. Osakada, T. Laoui, Rapid manufacturing of metal components by laser forming, International Journal of Machine Tools and Manufacture 46(12-13) (2006) 1459-1468.

Scope of Study - Detailed Analysis of DMLS Structure & Properties

- Detailed literature review-microstructure and properties of IN718
- Investigation of active creep mechanisms in wrought and DMLS IN718
- Microstructural analysis of DMLS and wrought IN718
- Preliminary thermal modeling of DMLS processing

Nickel Base Superalloys Offer Superior Properties Through Complex Microstructural Systems

Limiting Chemical Composition[a], %	
Nickel (plus Cobalt)	50.00-55.00
Chromium	17.00-21.00
Iron	Balance*
Niobium (plus Tantalum)	4.75-5.50
Molybdenum	2.80-3.30
Titanium	0.65-1.15
Aluminum	0.20-0.80
Cobalt	1.00 max.
Carbon	0.08 max.
Manganese	0.35 max.
Silicon	0.35 max.
Phosphorus	0.015 max.
Sulfur	0.015 max.
Boron	0.006 max.
Copper	0.30 max.

[a]Conforms to AMS specifications

*Reference to the 'balance' of a composition does not guarantee this is exclusively of the element mentioned but that it predominates and others are present only in minimal quantities.

Composition of IN718 Source: SpecialMetals, Inconel alloy 718.

Phase	Prototype	Pearson symbol	Strukturbericht symbol	Lattice [nm]	Chemical Composition (Appx)
γ'	Cu_3Au	cP4	$L1_2$	a 0.36	$(Ni\ Co)_3(Al\ Ti)$
γ''	Al_3Ti	tI8	$D0_{22}$	a 0.36 c 0.74	$(Ni\ Fe)_3(Nb\ Al\ Ti)$
MC	NaCl	cF8	B1	a 0.44	(Ti Ta)C or TiC, TaC, NbC, WC
M_6C	Fe_3W_3C	cF112	$E9_3$	a 1.11	$(Mo\ Cr\ W)_6C$
M_7C_3	Cr_7C_3	oP40	$D10_1$	a 0.45 b 0.70 c 1.21	Cr_7C_3
$M_{23}C_6$	$Cr_{23}C_6$	cF116	$D8_4$	a 1.07	$Cr_{21}Mo_2C_6$
M_5B_3	Cr_5B_3	tI32	$D8_1$	a 0.55 c 1.06	$(Cr\ Mo)_5B_3$
M_3B_2	Si_2U_3	tP10	$D5_a$	a 0.60 c 0.32	$(Mo\ Cr)_3B_2$
σ	CrNi	tP30	$D8_b$	a 0.88 c 0.46	Cr Mo Co based
δ	Cu_3Ti (β)	oP8	$D0_a$	a 0.51 b 0.43 c 0.46	Ni_3Nb
η	Ni_3Ti	hP16	$D0_{24}$	a 0.51 c 0.83	$Ni_3(Ti\ Ta)$
μ	Fe_7W_6	hR13	$D8_5$	a 0.48 c 2.5	Mo Co based

Table 1. Summary of second phases in the polycrystalline Ni based superalloys [10] The lattice parameter may vary (less than 5%) by changing chemical composition.

Phases of IN718 Source:
H. Kitaguchi, Microstructure-Property Relationship in Advanced Ni-Based Superalloys, 2012.

Optimized Processing Developed for IN718

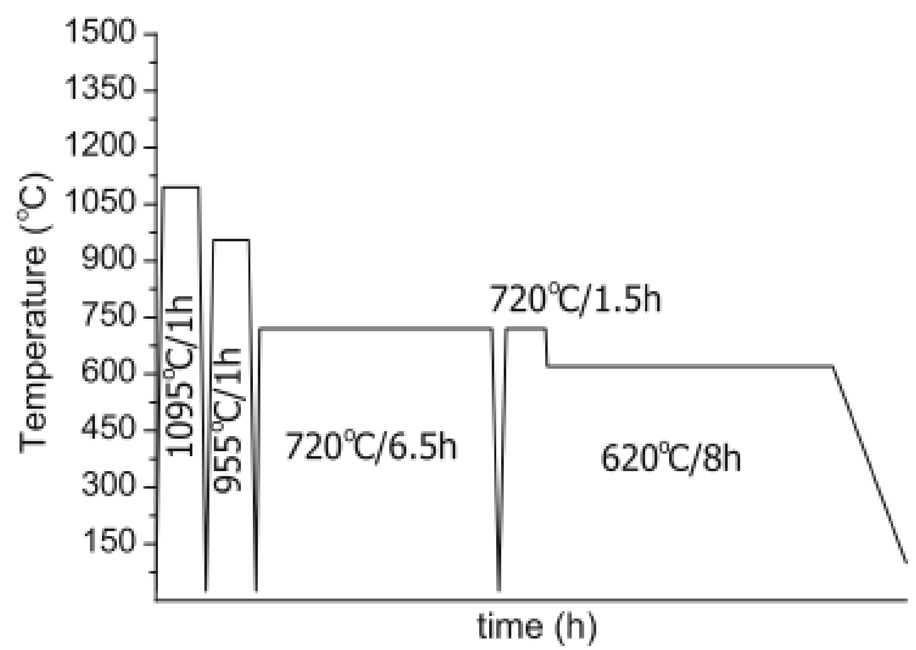

Double aging heat treatment applied on Inconel 718

Heat treatment process in IN718 Source:
Caliari, Felipe Rocha et al. "Effect of Double Aging Heat Treatment on the Short-Term Creep Behavior of the Inconel 718." *Journal of Materials Engineering and Performance*, vol. 25, no. 6, 2016, pp. 2307-2317, doi:10.1007/s11665-016-2051-2.

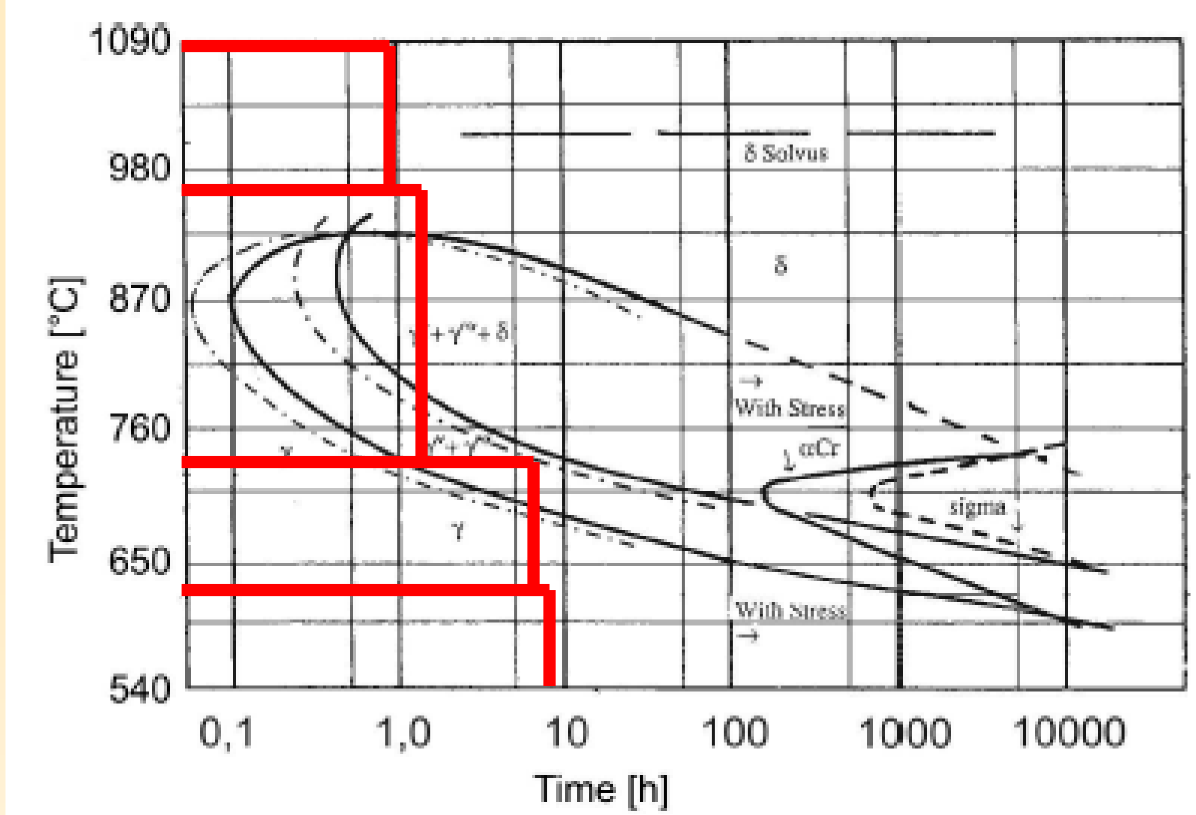

TTT diagrams of IN718, the dash-dot curves are the modification for forging at high strain rates reported by the investigators Source: Oradei-Basile, Armida and John F Radavich. "A Current Ttt Diagram for Wrought Alloy 718." *Superalloys*, vol. 718, no. 625, 1991, pp. 325-335.

Optimized Processing of IN718 is Developed to Avoid Formation of Detrimental Laves Phase

- Laves phase undesirable
- Rapid cooling leads to solid solution and avoids Laves phase

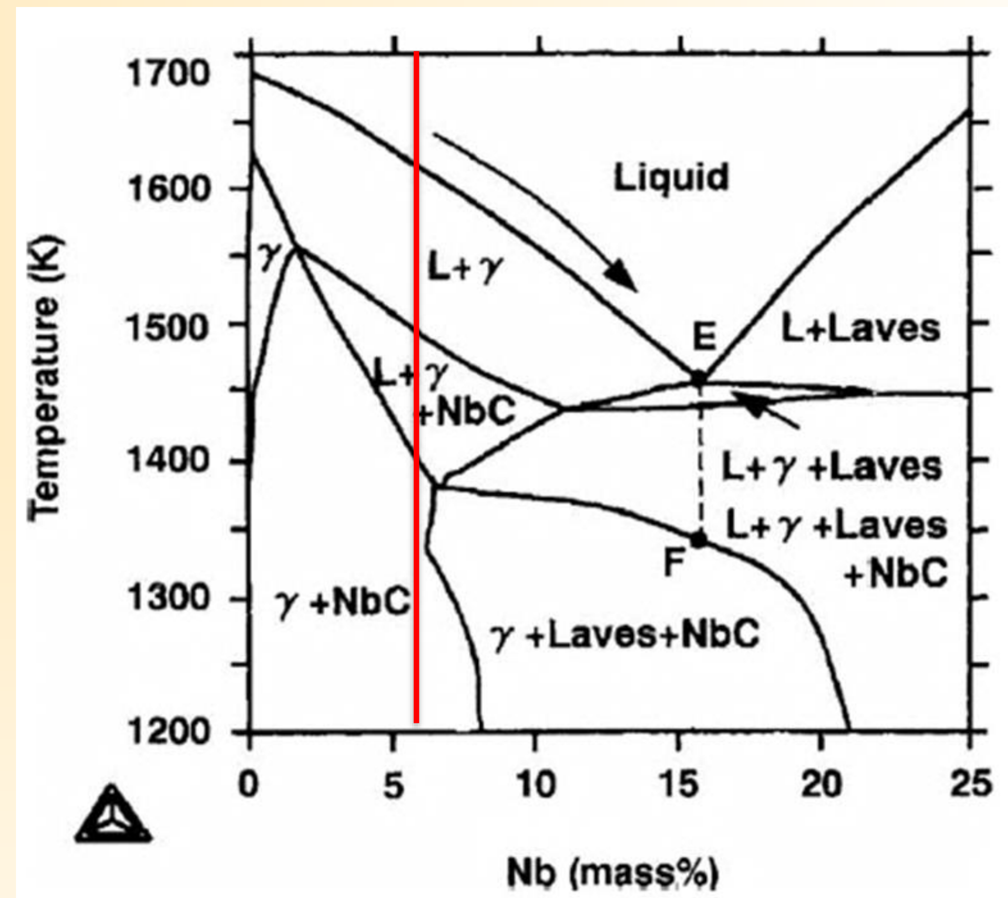

Phase diagram of Inconel 718 alloy Source: Oradei-Basile, Armida and John F Radavich. "A Current Ttt Diagram for Wrought Alloy 718." *Superalloys*, vol. 718, no. 625, 1991, pp. 325-335.

Preferred Orientation and Texturing is Developed During Additive Manufacturing

Columnar/Epitaxial Growth

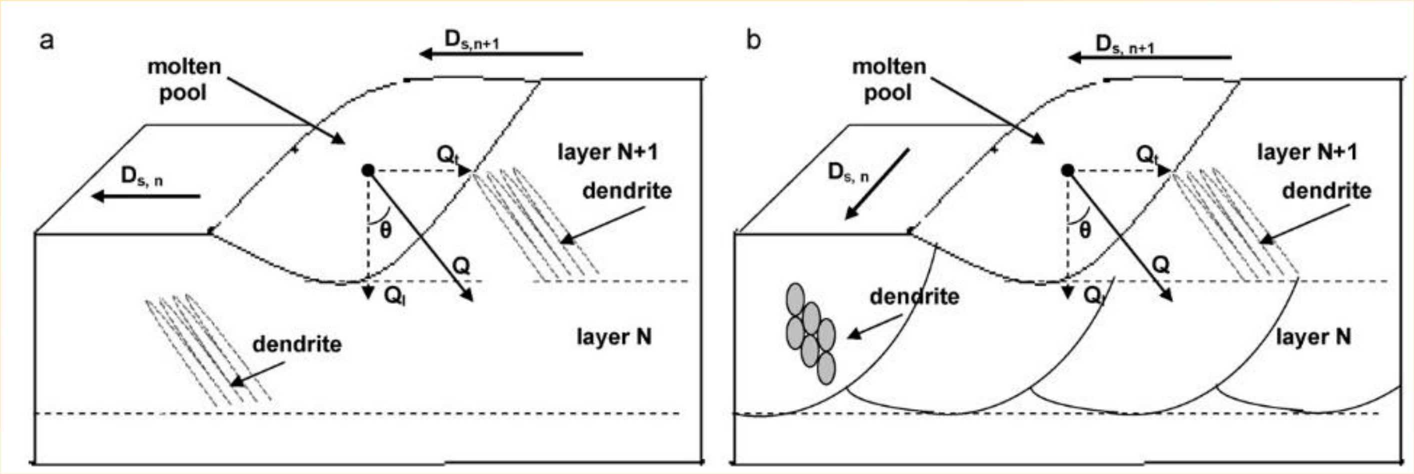

Schematic plans of heat dissipation and dendrites growth when SDRS (a) and CDRS (b) path patterns were adopted. Q represents the heat dissipation direction, and Qt,Ql represent the transverse dissipation and longitudinal dissipation of heat respectively. Ds,n represents the laser scanning direction in layer N, as well as the Ds,n+1. Source:
Liu, Fencheng et al. "The Effect of Laser Scanning Path on Microstructures and Mechanical Properties of Laser Solid Formed Nickel-Base Superalloy Inconel 718." *Journal of Alloys and Compounds*, vol. 509, no. 13, 2011, pp. 4505-4509, doi:10.1016/j.jallcom.2010.11.176.

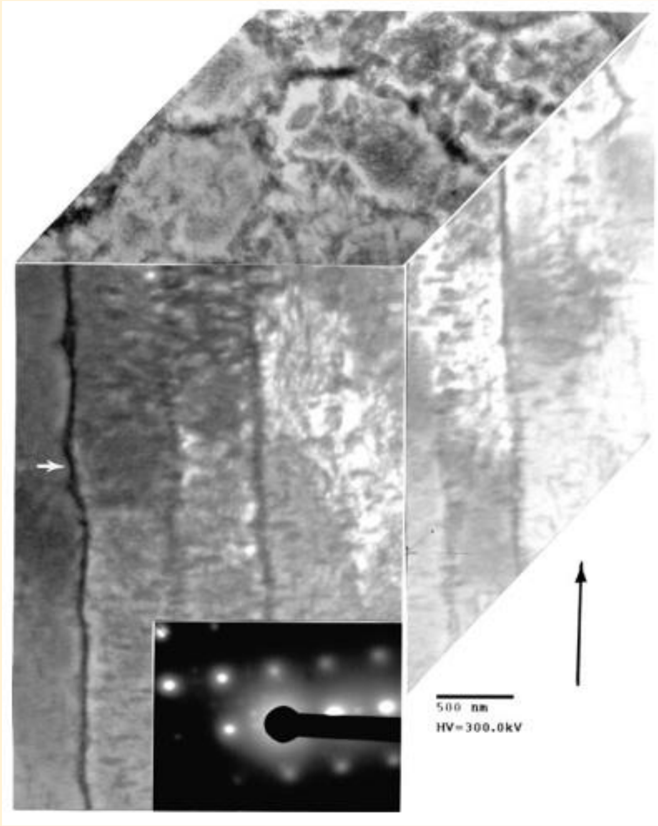

3-D TEM image composite view for an as-fabricated (in argon) z axis cylinder HIP in argon. (Inset) The SAED pattern corresponds to a c[001] zone in the vertical reference plane, as shown. The arrow to the right indicates the build direction. Source:
Amato, K. N. et al. "Microstructures and Mechanical Behavior of Inconel 718 Fabricated by Selective Laser Melting." *Acta Materialia*, vol. 60, no. 5, 2012, pp. 2229-2239, doi:10.1016/j.actamat.2011.12.032.

Microstructural Features developed in IN718 are Influence by Stress

- Tension leads to γ''
- Compression leads to γ'
- Tension strengthens more than compression weakens as compared to non-stress aged IN718

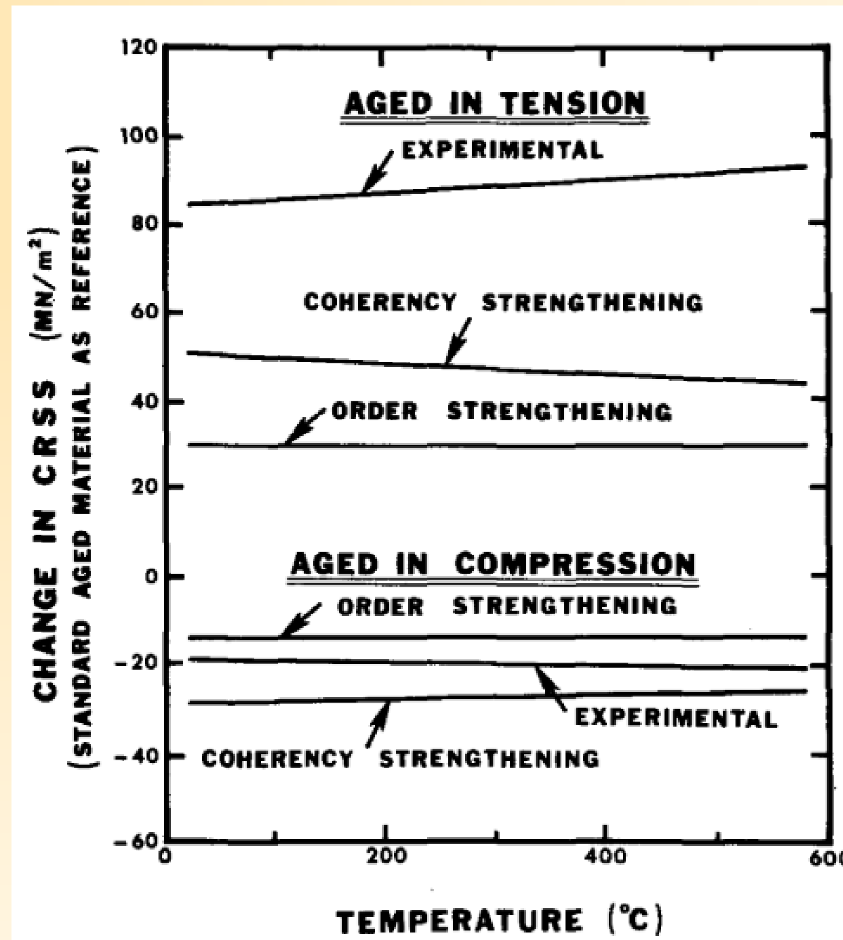

Differences in CRSS between [001] crystals ages under stress and aged without stress. Source: Oblak, J. M. et al. "Coherency Strengthening in Ni Base Alloys Hardened by Do22 Γ′ Precipitates." *Metallurgical Transactions*, vol. 5, no. 1, 1974, p. 143, doi:10.1007/bf02642938.

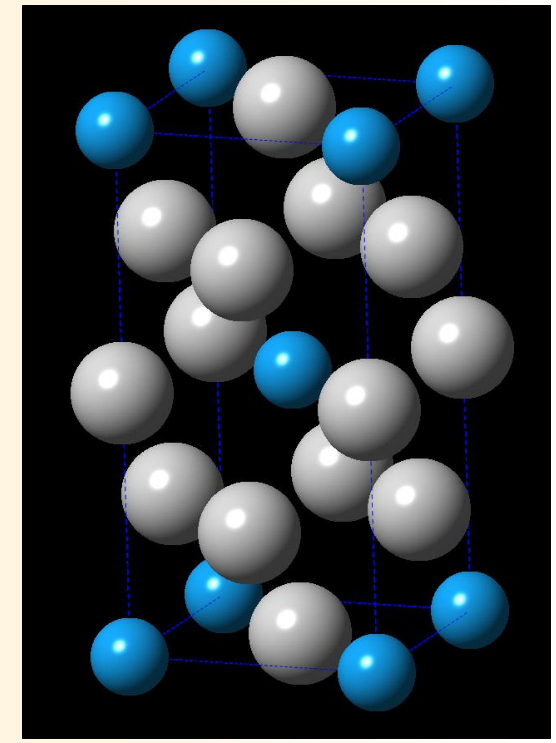

$\gamma''model$

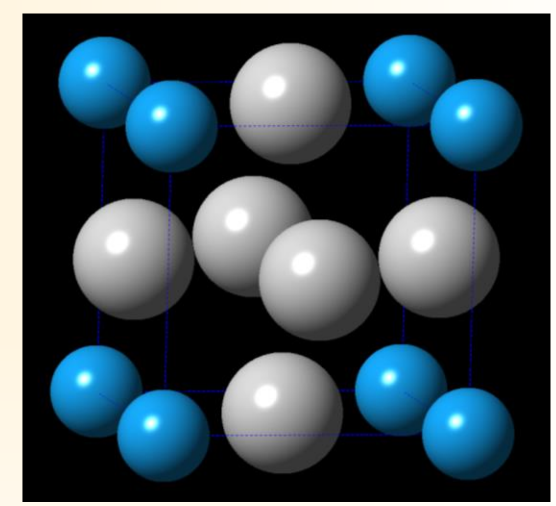

$\gamma'model$

Internal Stress Developed due Rapid Cooling in DMLS Can Lead to Different Microstructure

- γ'' phase can be grown and isolated via heat treatments and stress
- Strong columnar texturing occurs as a result of solidification conditions
- Mixed stresses during ageing have an overall positive effect on strengthening

Creep Data Were Analyzed in Quest to Better Understand the Differences the Observed Behavior

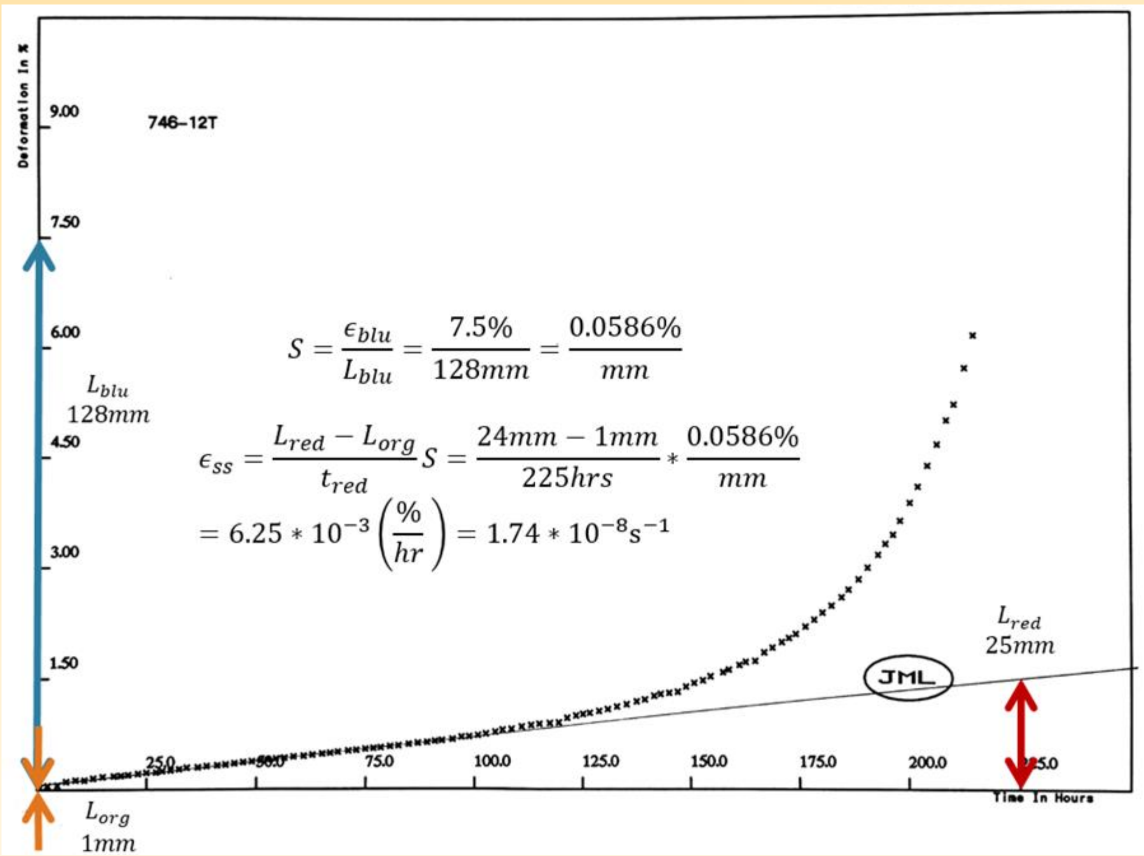

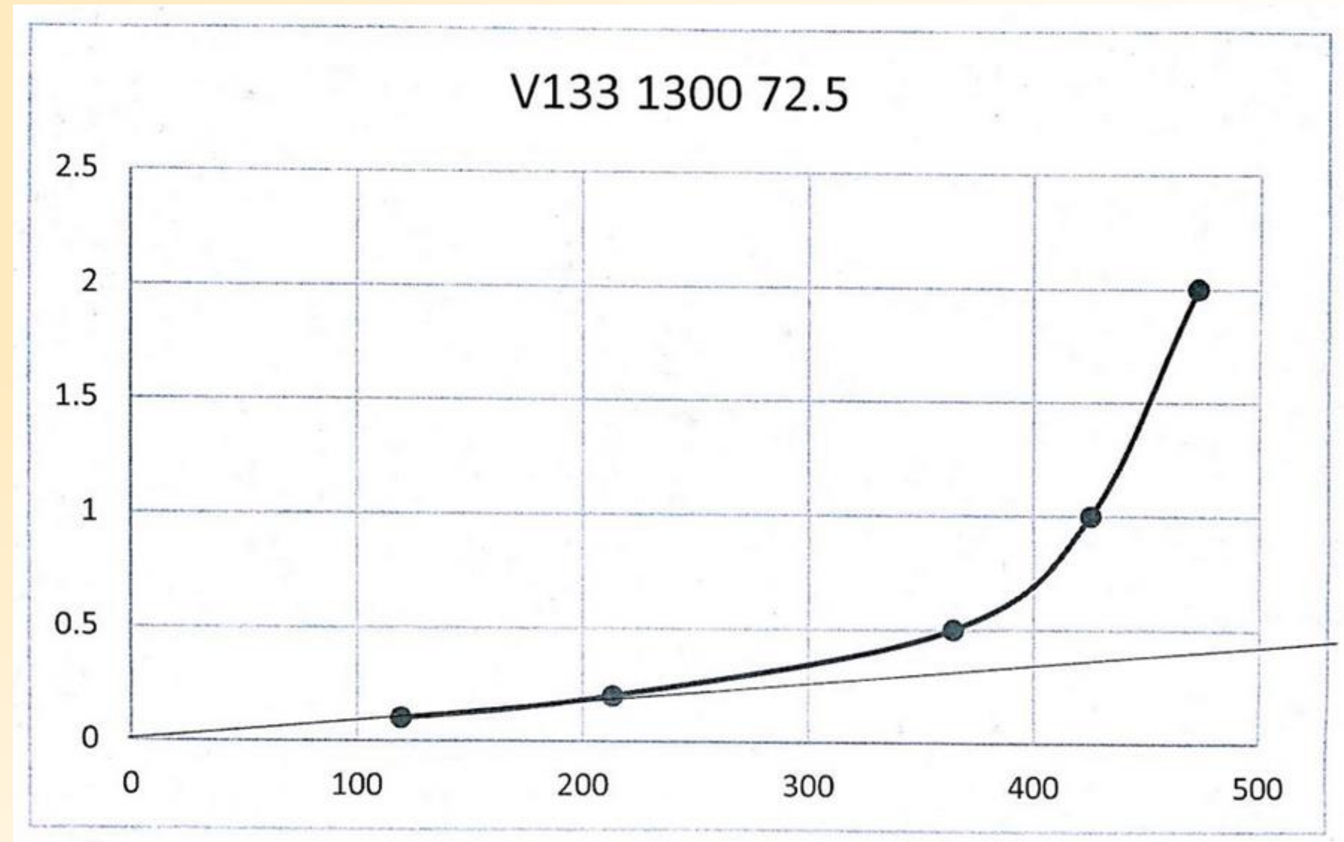

Steady-State Creep determination based on creep rupture curves for conventional and DMLS IN718

Creep Deformation Used in Modeling the Behavior in both Materials

$$\sigma_n = \frac{\sigma}{E(T)} \; (Eq.2)$$

$$\dot{\varepsilon}_{ss} = A(\sigma_n{}^n) \exp\left(-\frac{Q}{RT}\right) \; (Eq.3a)$$

$$\dot{\varepsilon}_{ss} = A[\sinh(B\sigma_n)\,]^n \; \exp\left(-\frac{Q}{RT}\right) \; (Eq.3b)$$

$$\ln(\dot{\varepsilon}_{SS}) = \ln(A) + n[\ln(\sinh(B\sigma_n))] - \left(\frac{Q}{RT}\right) \; (Eq.4b)$$

Difference in Active Creep Mechanism in DMLS & Wrought Noted

Mechanism Change in Wrought Samples

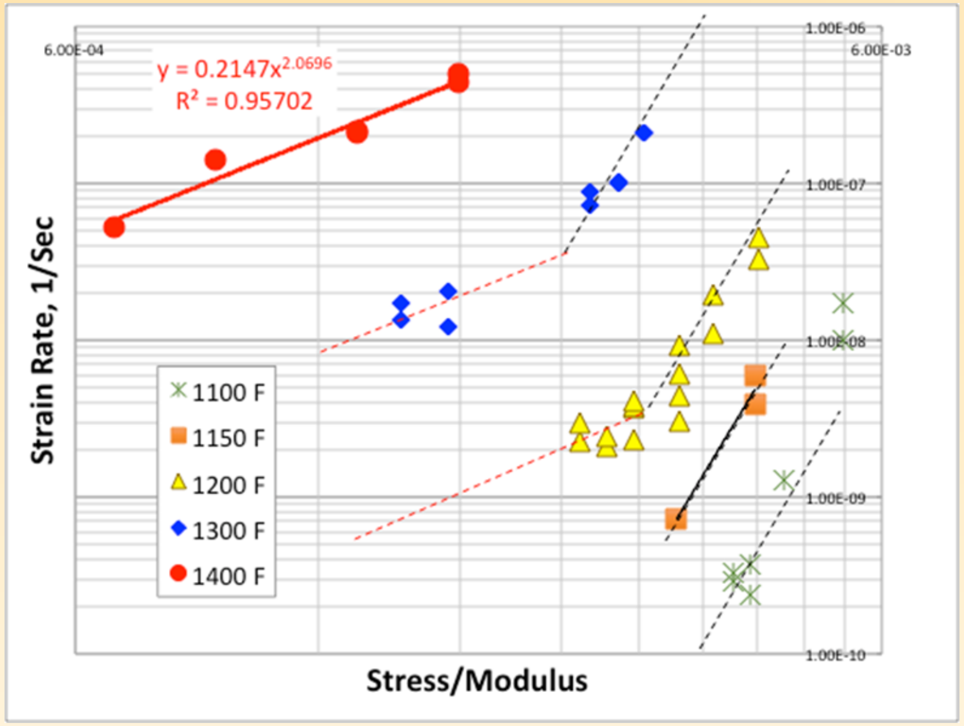

Log-log plot of strain rate of wrought IN718 for a range of temperatures and stresses. The stress component is normalized using the Young's modulus, it can be seen from the data trend that a departure in creep mechanism occurs in the 1200 and $1300^{o}F$ samples

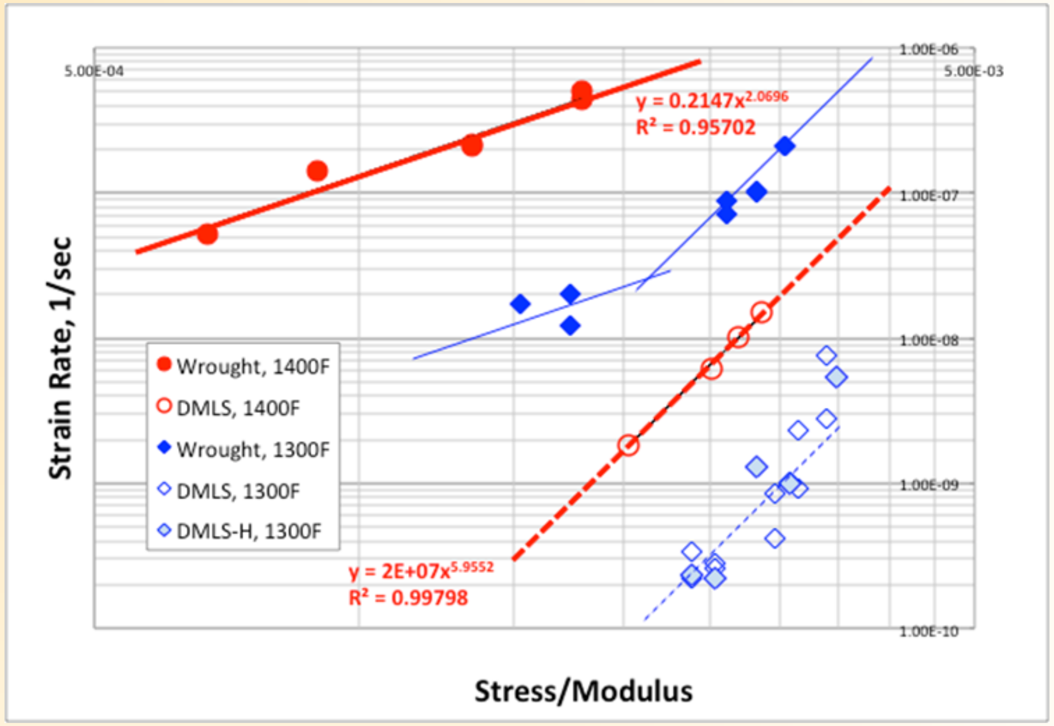

Combined data from Wrought and DMLS samples

DMLS Process Orientation has Minor effect on Creep Deformation

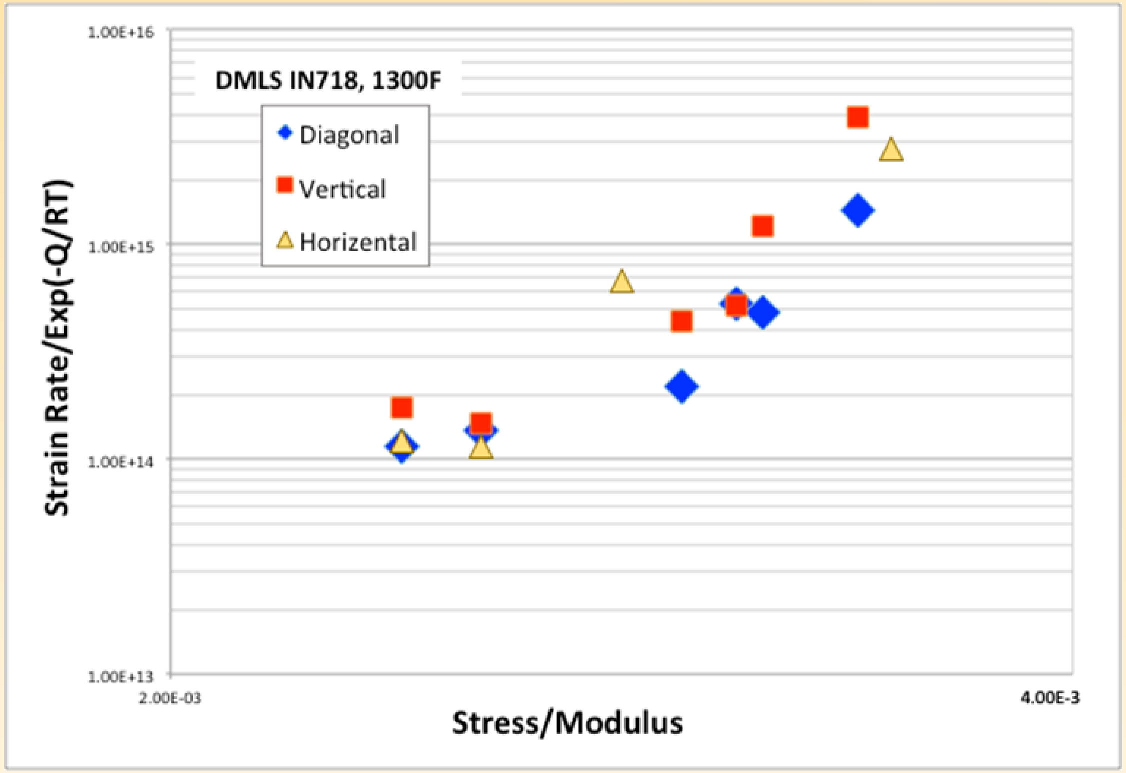

Effect of DMLS specimen orientation on creep behavior and illustration of orientation

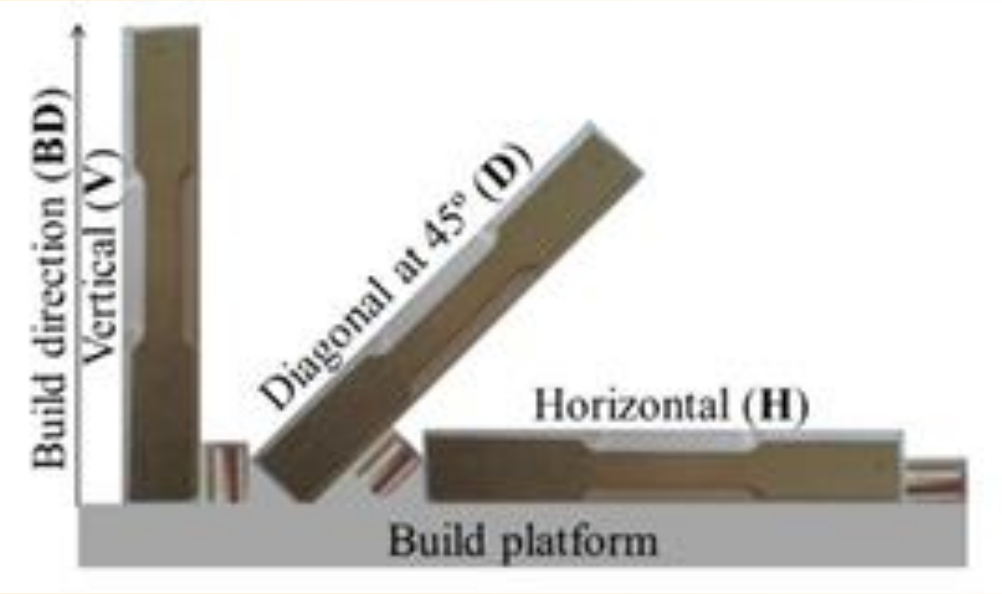

Illustration of specimen orientation Source: Smith, Derek H. et al. "Microstructure and Mechanical Behavior of Direct Metal Laser Sintered Inconel Alloy 718." *Materials Characterization*, vol. 113, 2016, pp. 1-9, doi:http://dx.doi.org/10.1016/j.matchar.2016.01.003.

Stress and Temperature Effect on Creep Correctly Modeled

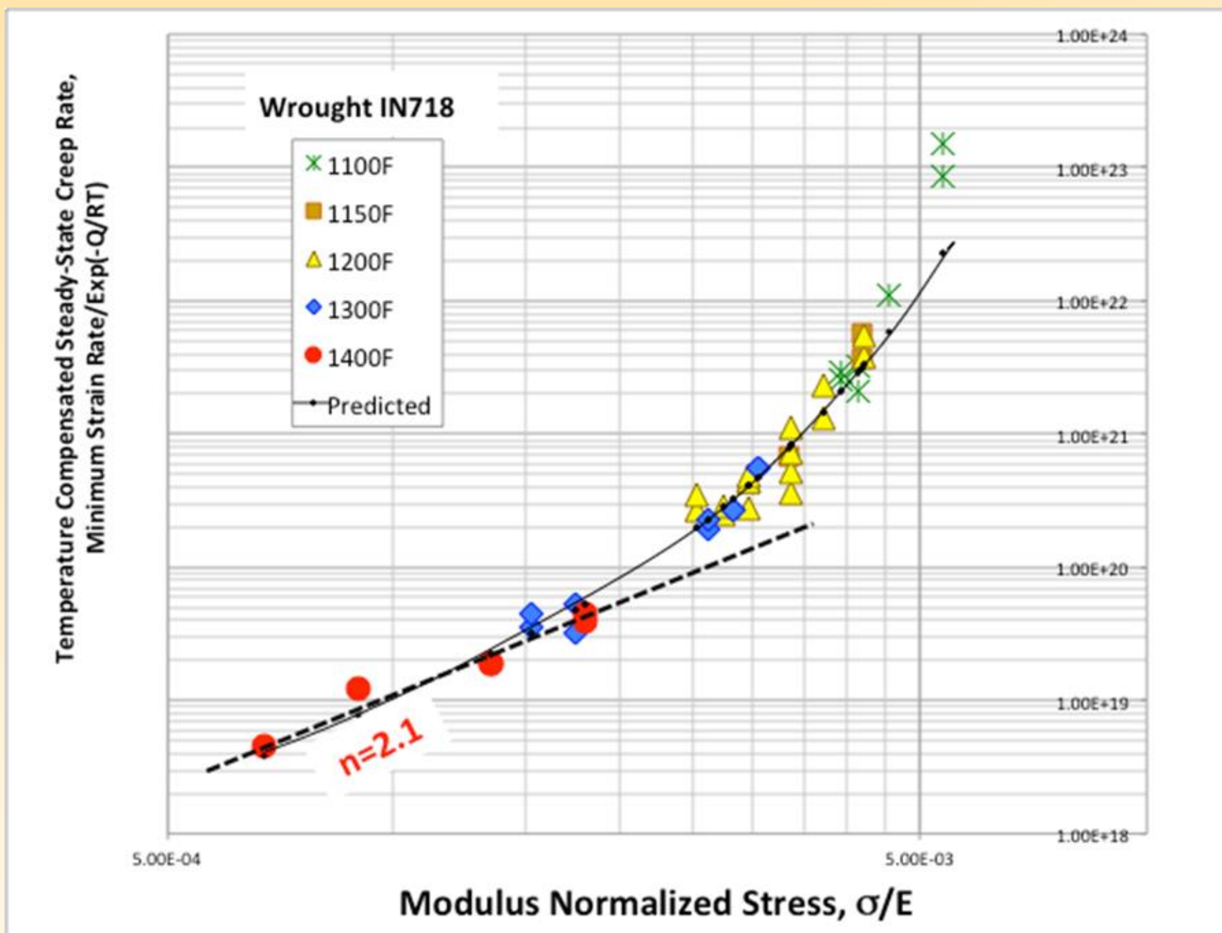

Steady state creep values for DMLS IN718 are shown in blue whith the fitted function illustrated as an orange curve

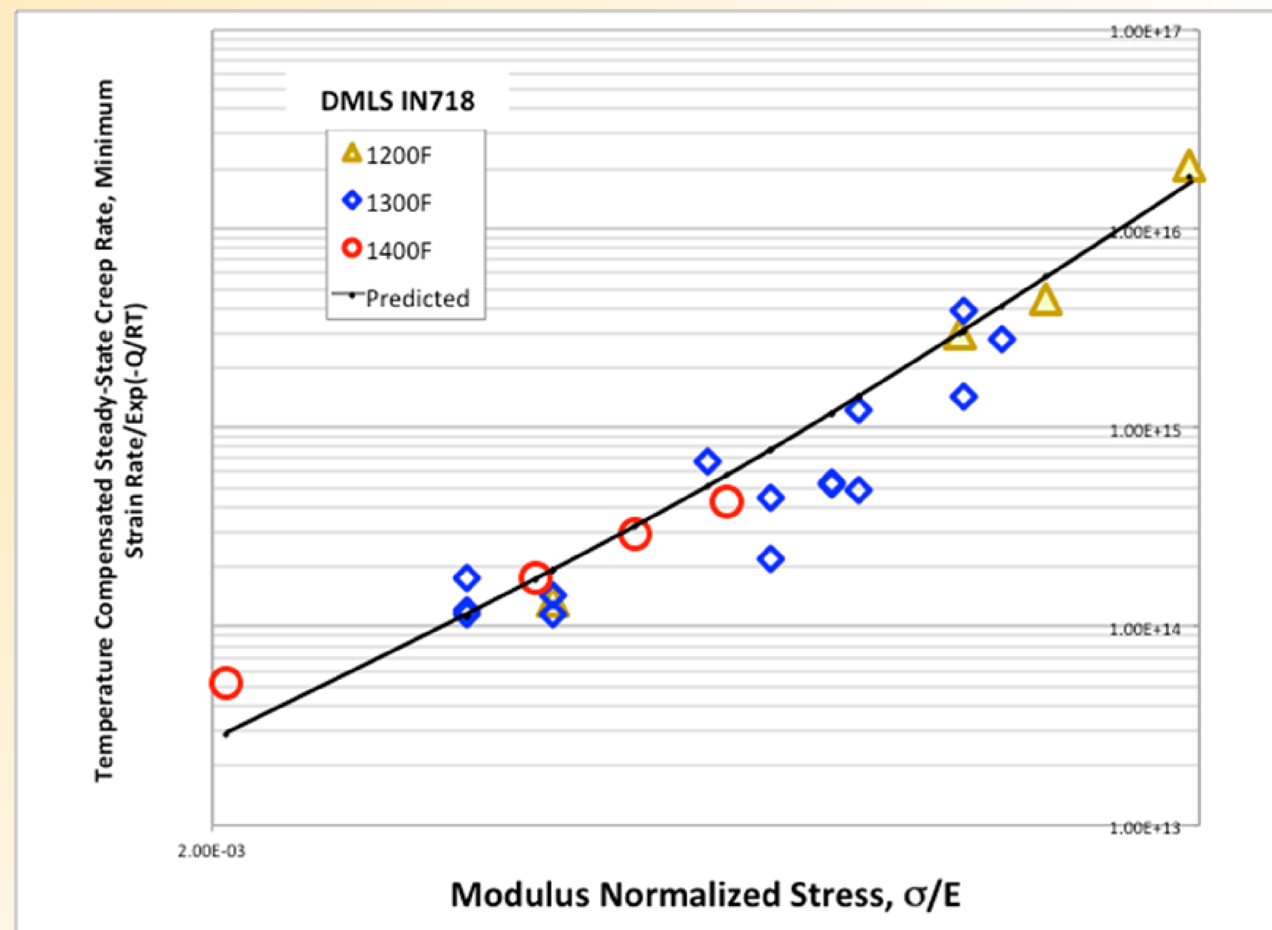

Plot of temperature-compensated steady state creep rates vs. normalized-stress for wrought and DMLS IN718 samples

Superior Creep Behavior in DMLS is Noted & Accurately Predicted by the Models

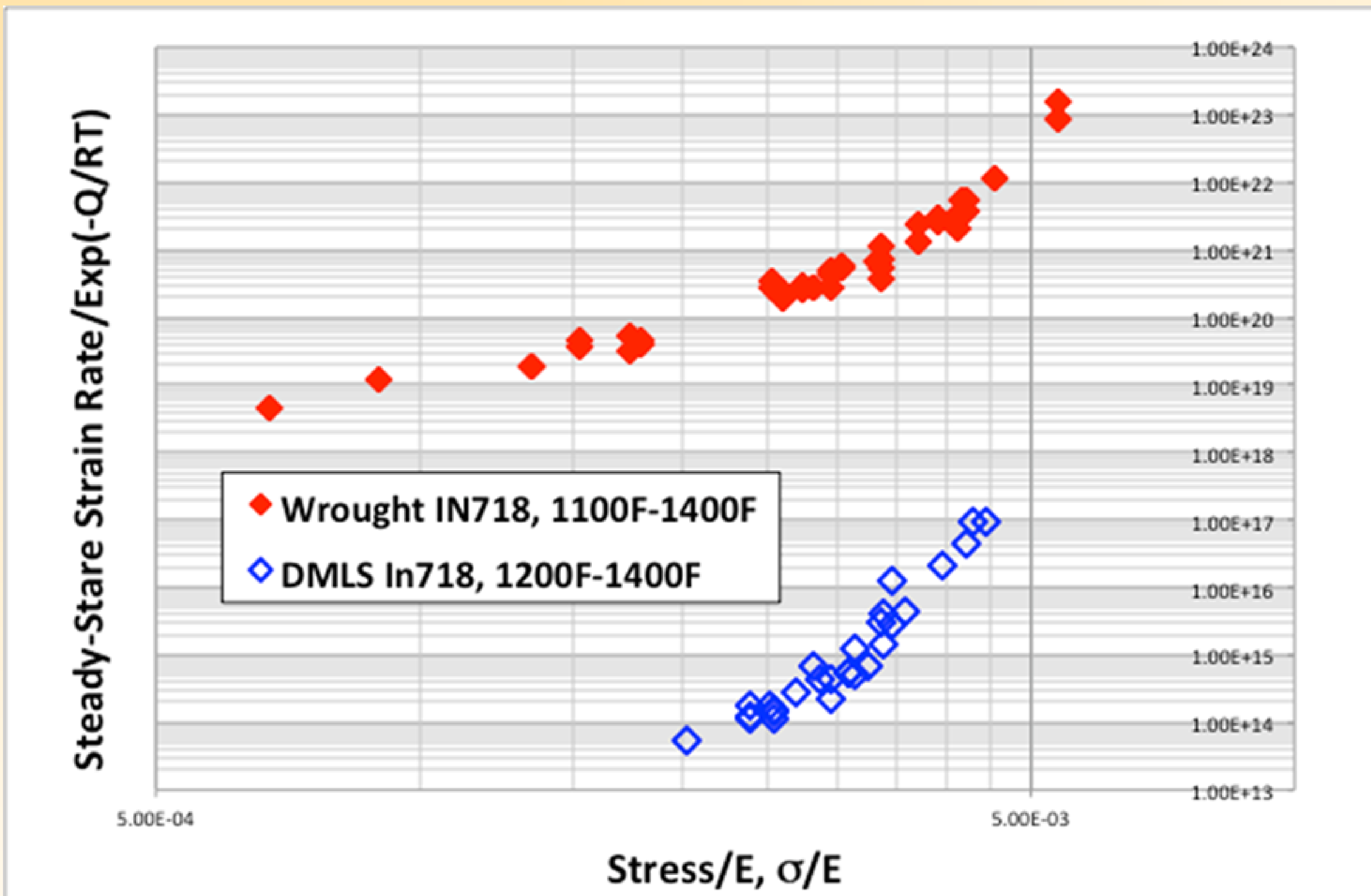

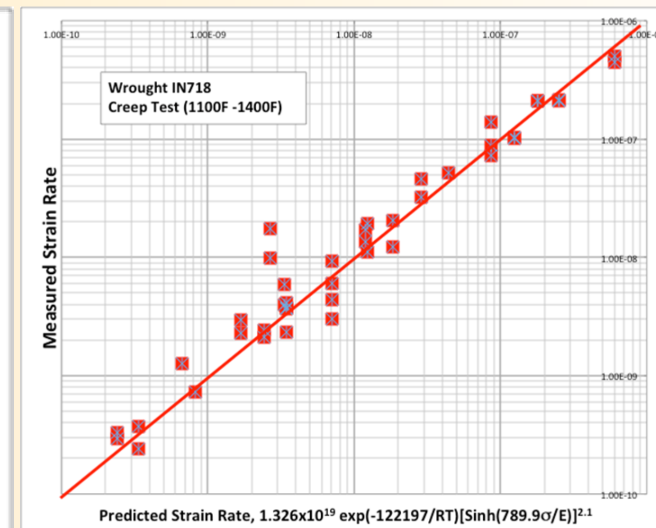

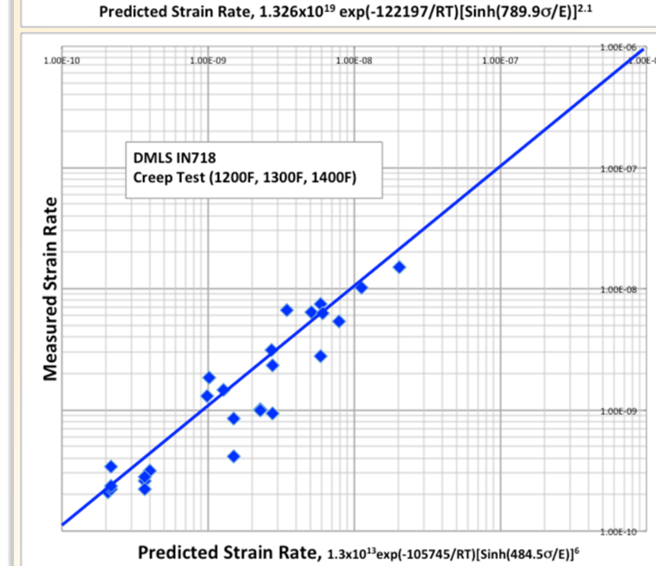

Temperature-compensated creep rate vs normalized stress for wrought and DMLS samples, plots of measured vs predicted creep rates for DMLS and wrought models

Summary of Creep Data Analysis Findings

- Wrought data shows a change in mechanism at high T
- DMLS doesn’t show any mechanism change for given range
- While the Q for DMLS was lower the “n” value is larger and points to diffusion or GB sliding, whereas the value for wrought points to a dislocation glide mechanism at high stress
- Both models appear to be statistically sound

Fracture Surface of DMLS Samples Shows Intergranular Failure

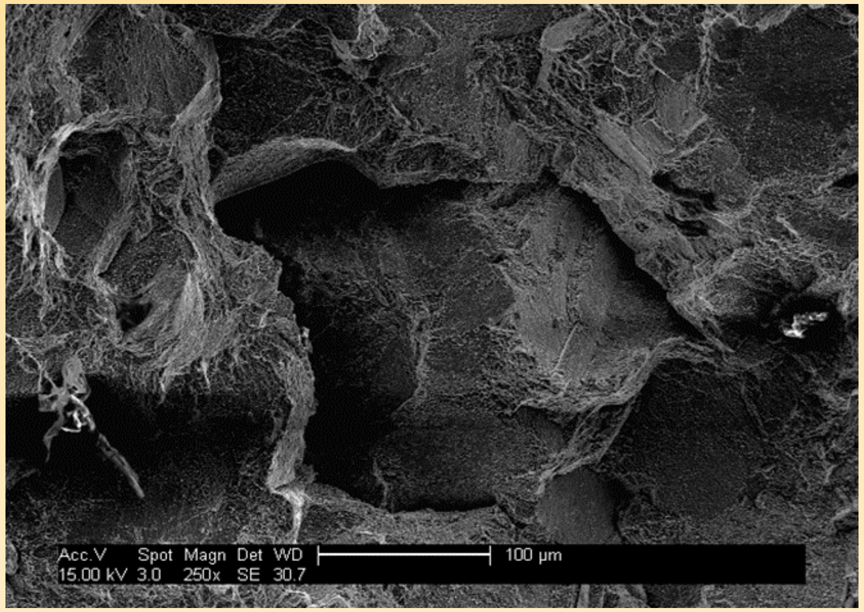

Fracture surface of V130 creep ruptured sample tested at 1300° F and 55ksi for 2796 hours

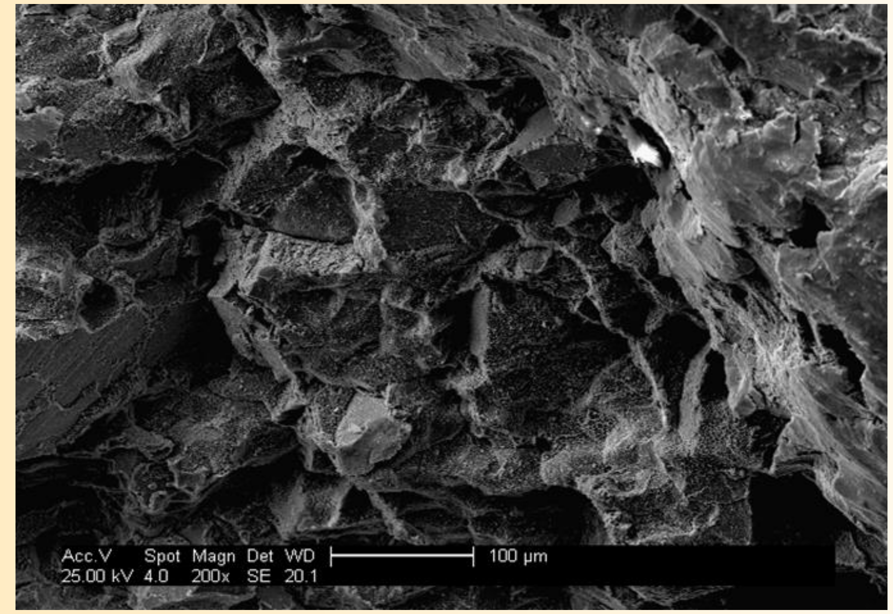

Fracture surface of H65 creep ruptured sample tested at 1300° F and 55ksi for 1918 hours

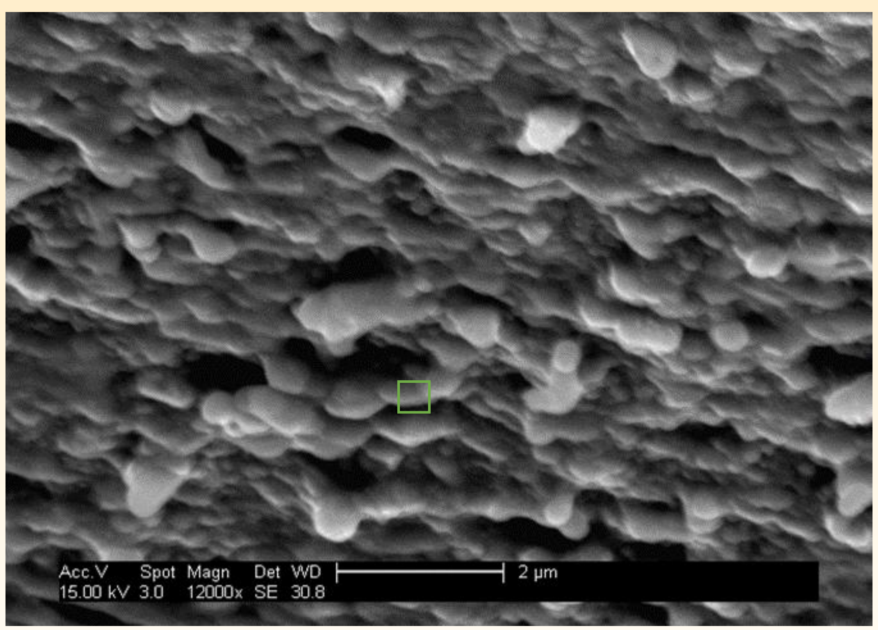

Surface of grain shown in figure above note the precipitate particles distributed throughout the surface

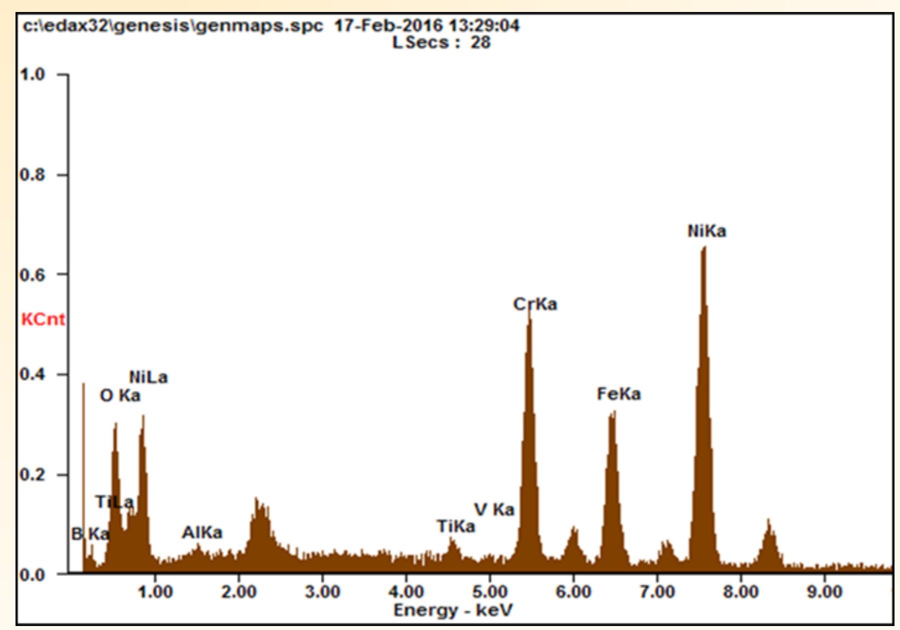

EDX analysis of the precipitate noted by box in image to the left

Build Orientation has an Effect on Fracture Morphology

- All cases show intergranular fracture
- Secondary phases/precipitates appear to be prevalent at grain boundaries
- Fracture appears to propagate from precipitates along grain boundaries
- Horizontal sample shows softer and less faceted surface

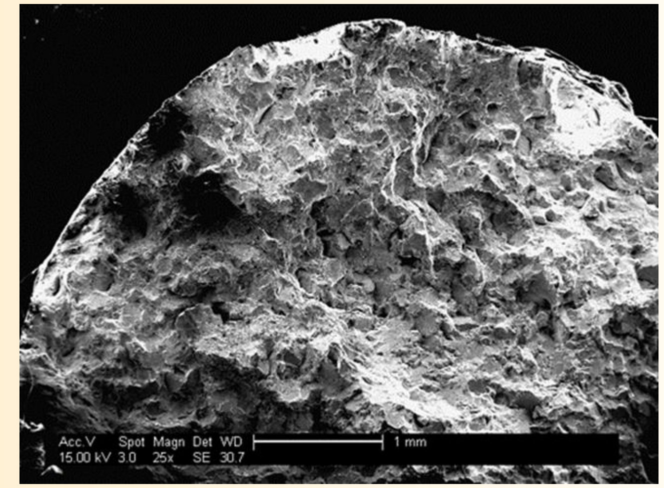

V130

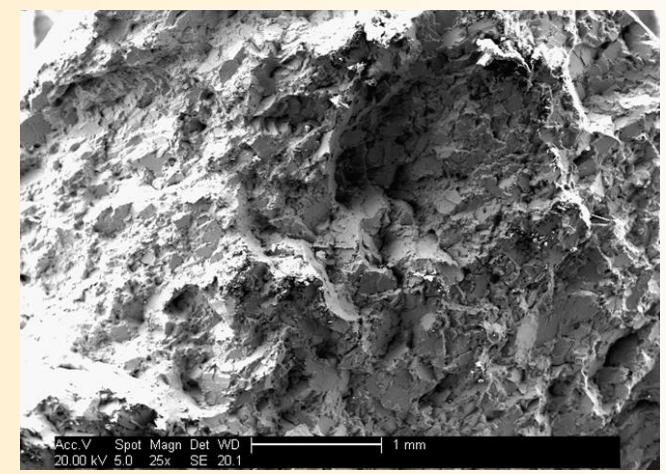

45-123

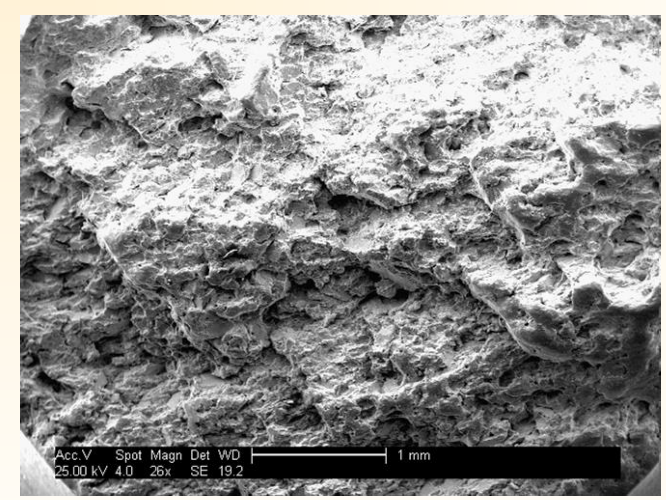

H65

Polished Samples Exhibit Precipitation Along Grain Boundaries and Homogenous γ'' Distribution

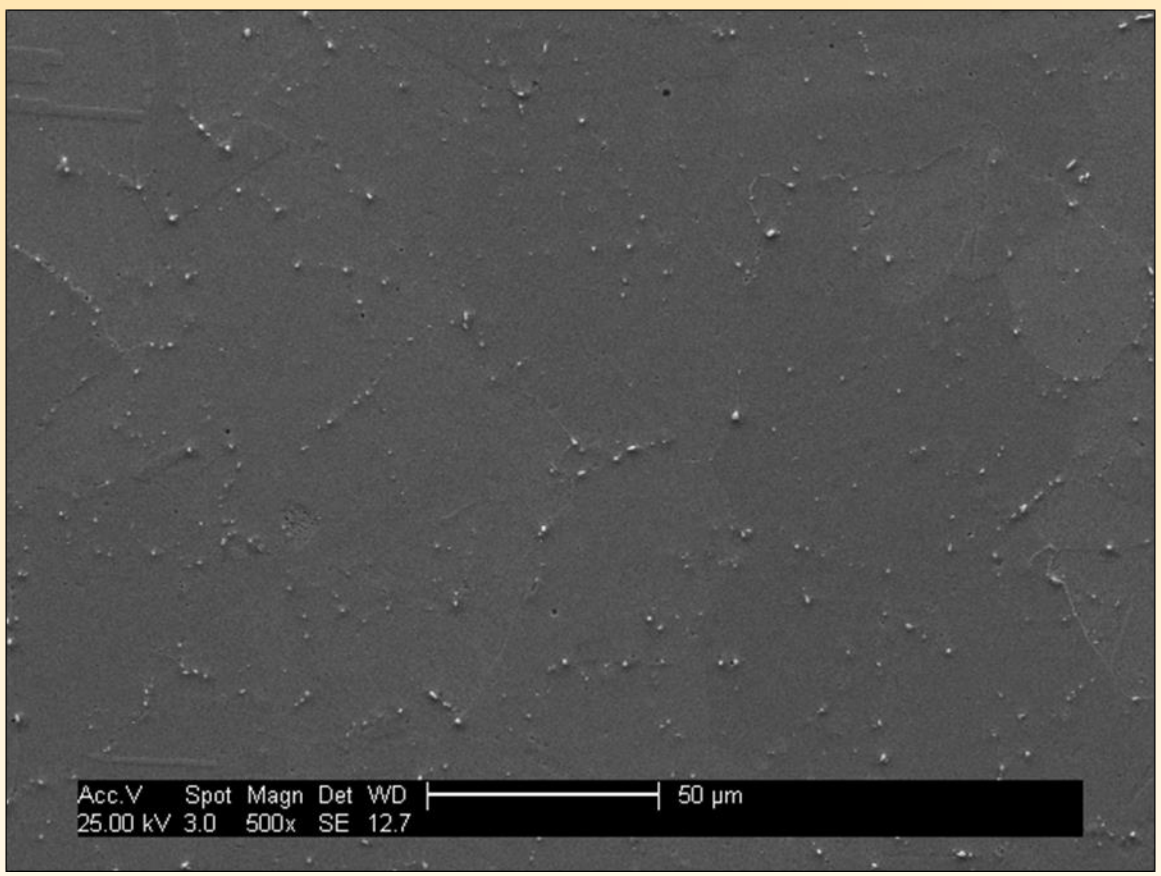

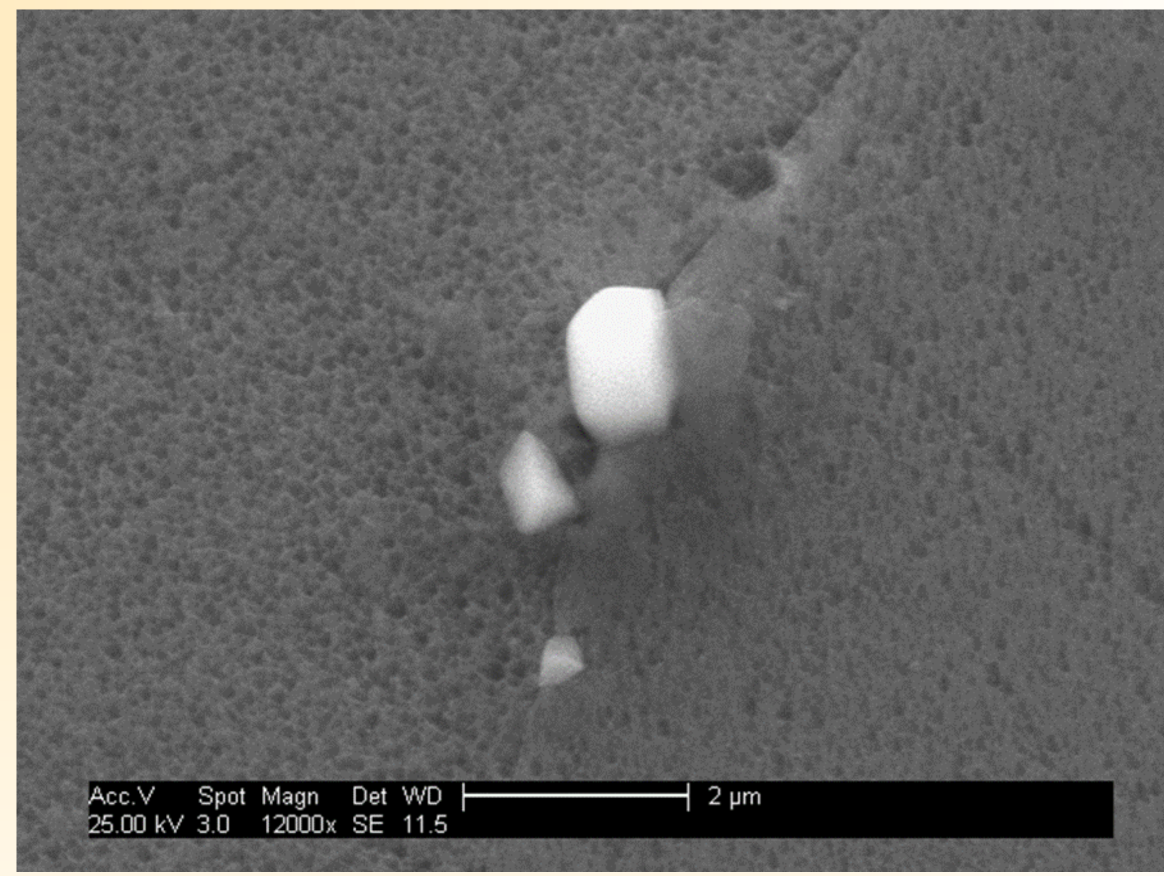

Images of sample 45-020 minor shade variations illustrate grain boundaries

EDX Analysis of Carbide and Oxide Impurities

- Creep rupture occurs along grain boundaries
- Precipitation of oxides and carbides appears to prefer grain boundaries
- Horizontal rupture surface appears softer and less grainy than vertical or 45 degree surfaces
- Pitting in polished surface suggests homogenous distribution γ'' and other secondary precipitates

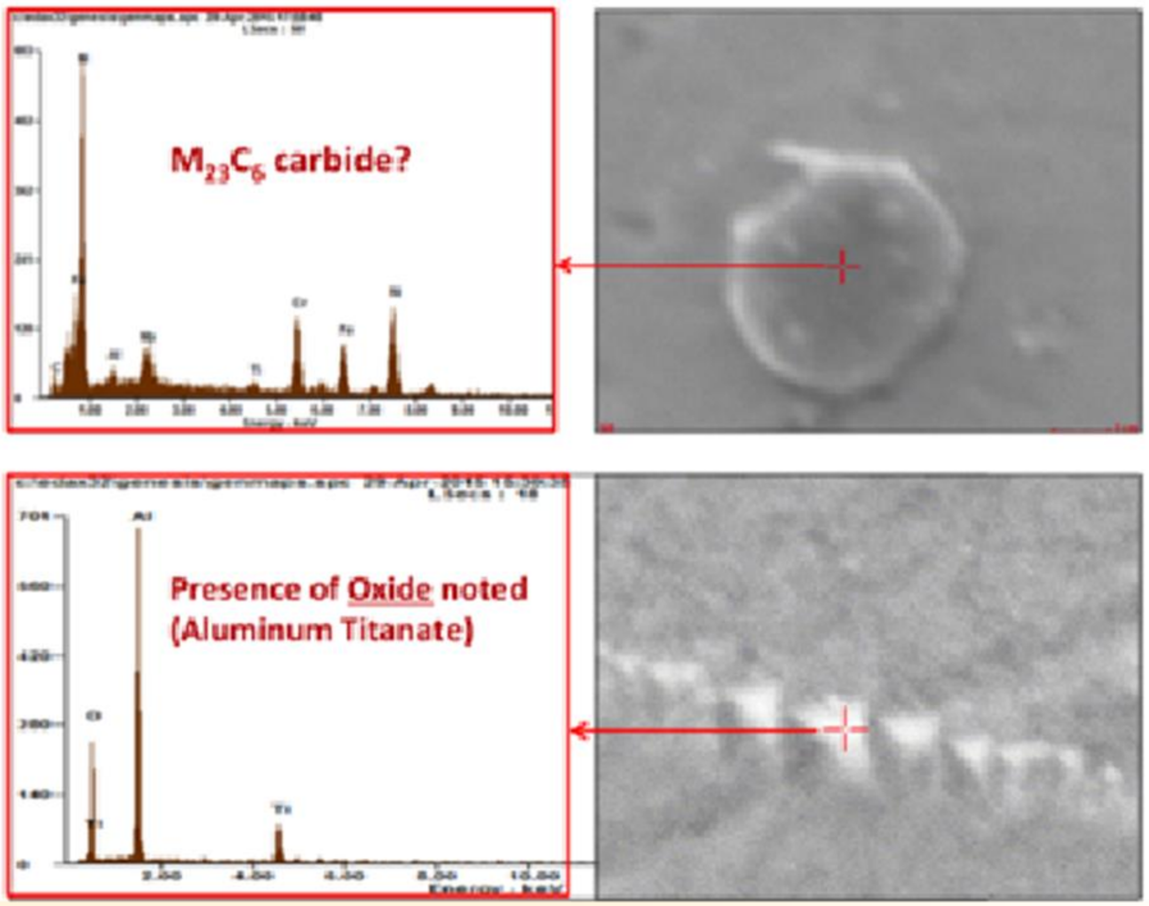

EDX analysis of precipitate on polished surface of a DMLS test-bar grip section

Sample Preparation using Electropolishing

- Preferred method for thinning superalloys is electropolishing
- Samples must be thinned to 100um or less
- E-Polishing had to be outsourced

Fischione Model 110 Twin-Jet Electropolisher
Source: Fischione. http://www.fischione.com/products/conventional-specimen-preparation/model-110-automatic-twin-jet-electropolisher. Accessed 1/30/2017.

40-42

Thinning and Polishing of Samples and Special Tools Created to Assist

- Samples cut using EDM
- Discs mounted using low-T wax
- Mounting assisted by weight system

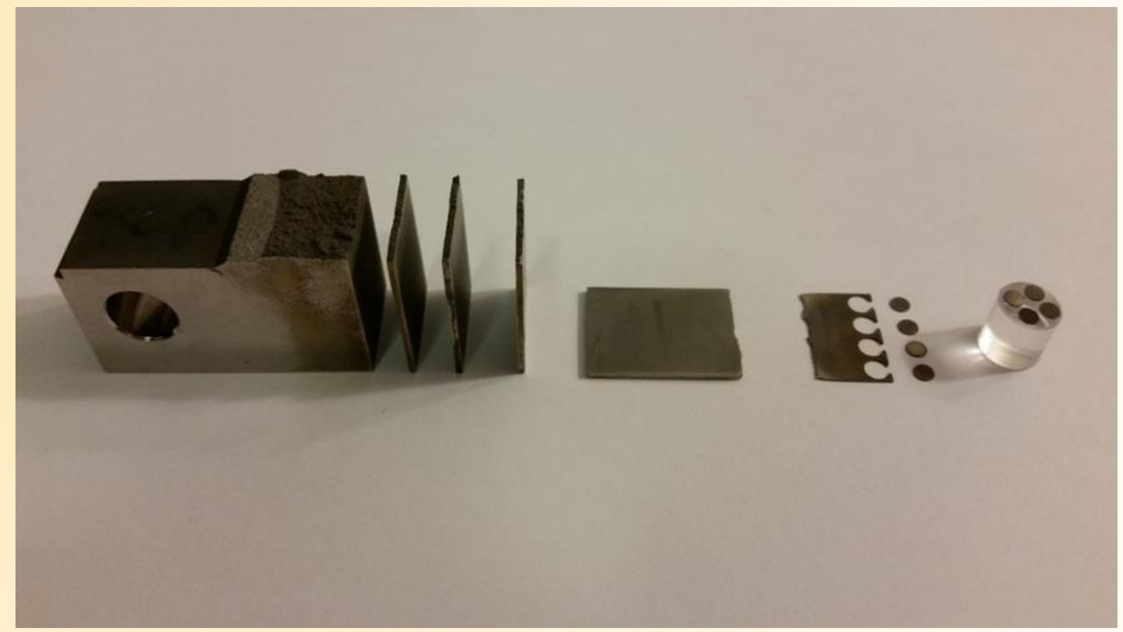

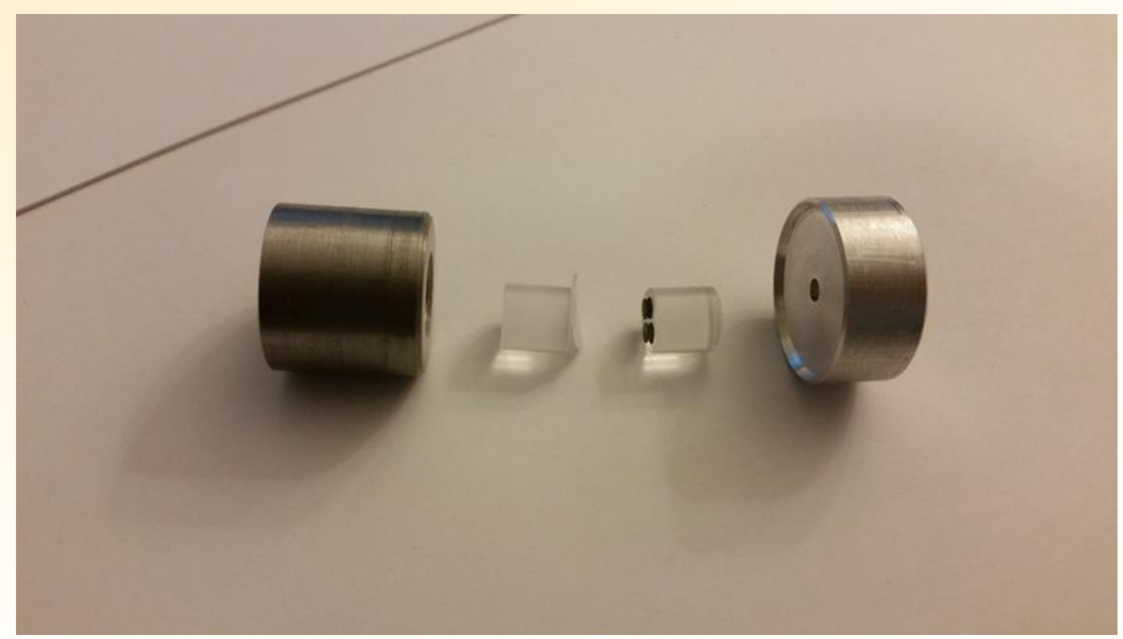

Secondary Phase Diffraction Modeling for TEM Identiication

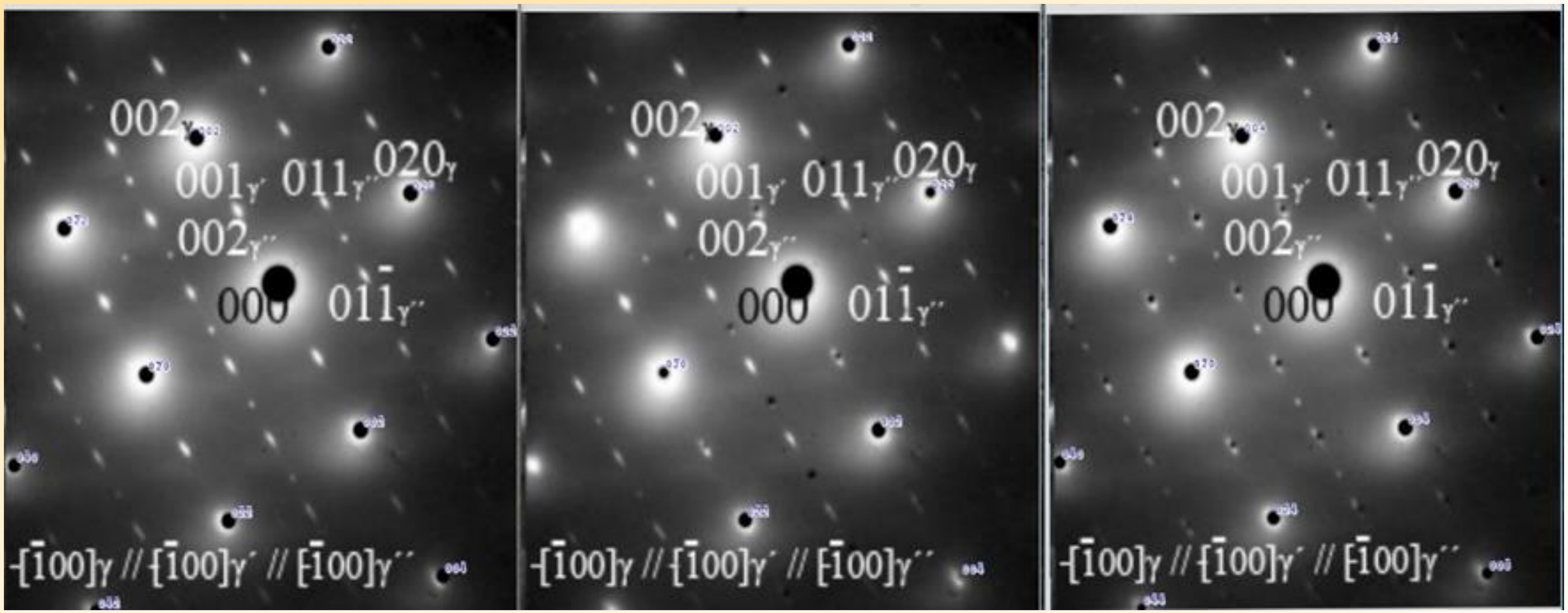

Simulated TEM diffraction patterns overlaid on an actual TEM diffraction pattern. From left to right the overlaid patters represent the $[\bar{1}\ 0\ 0]$ patterns for γ, γ', and γ'' phases.

TEM and STEM Imaging of Precipitation in DMLS IM718

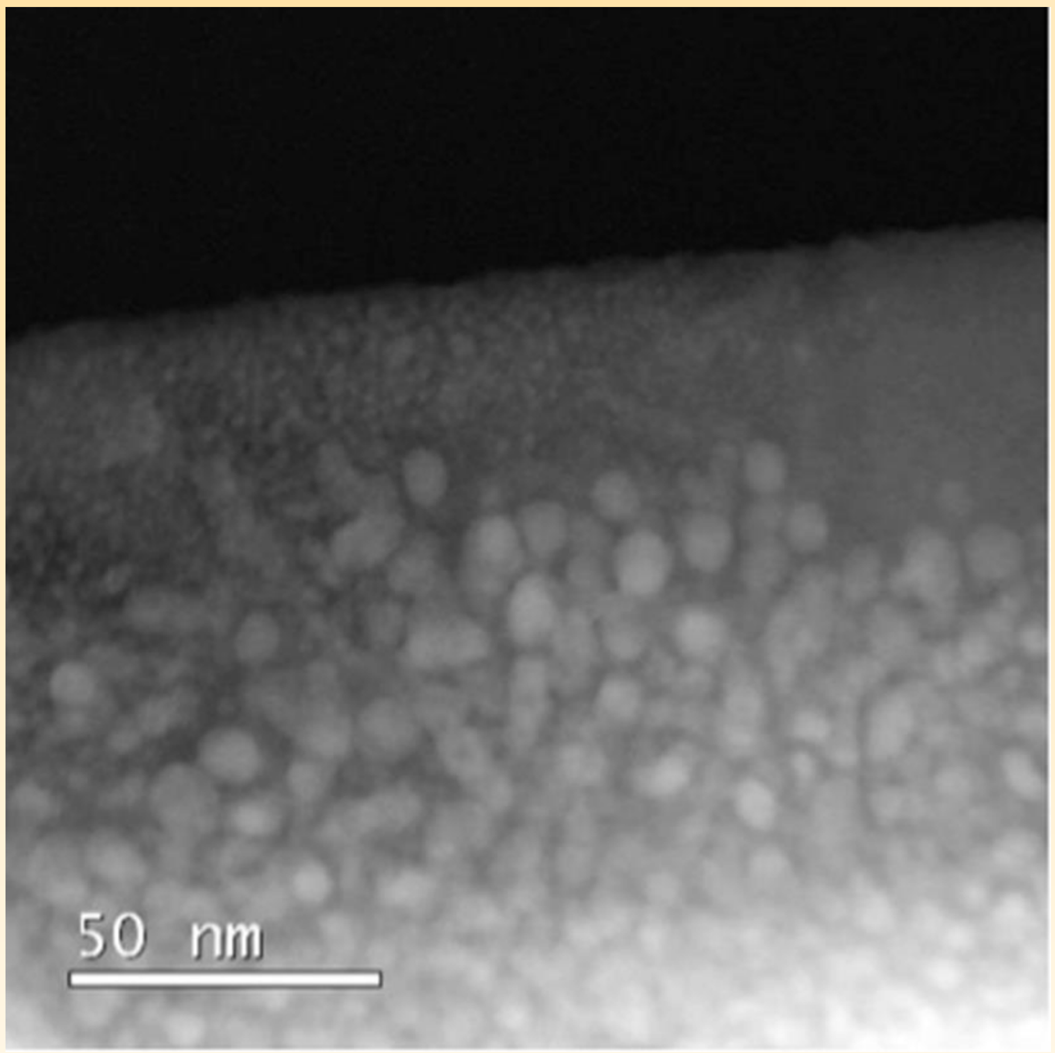

TEM analysis of FIB-prepared DMLS sample showing metastable γ''phase dispersed in a γ matrix

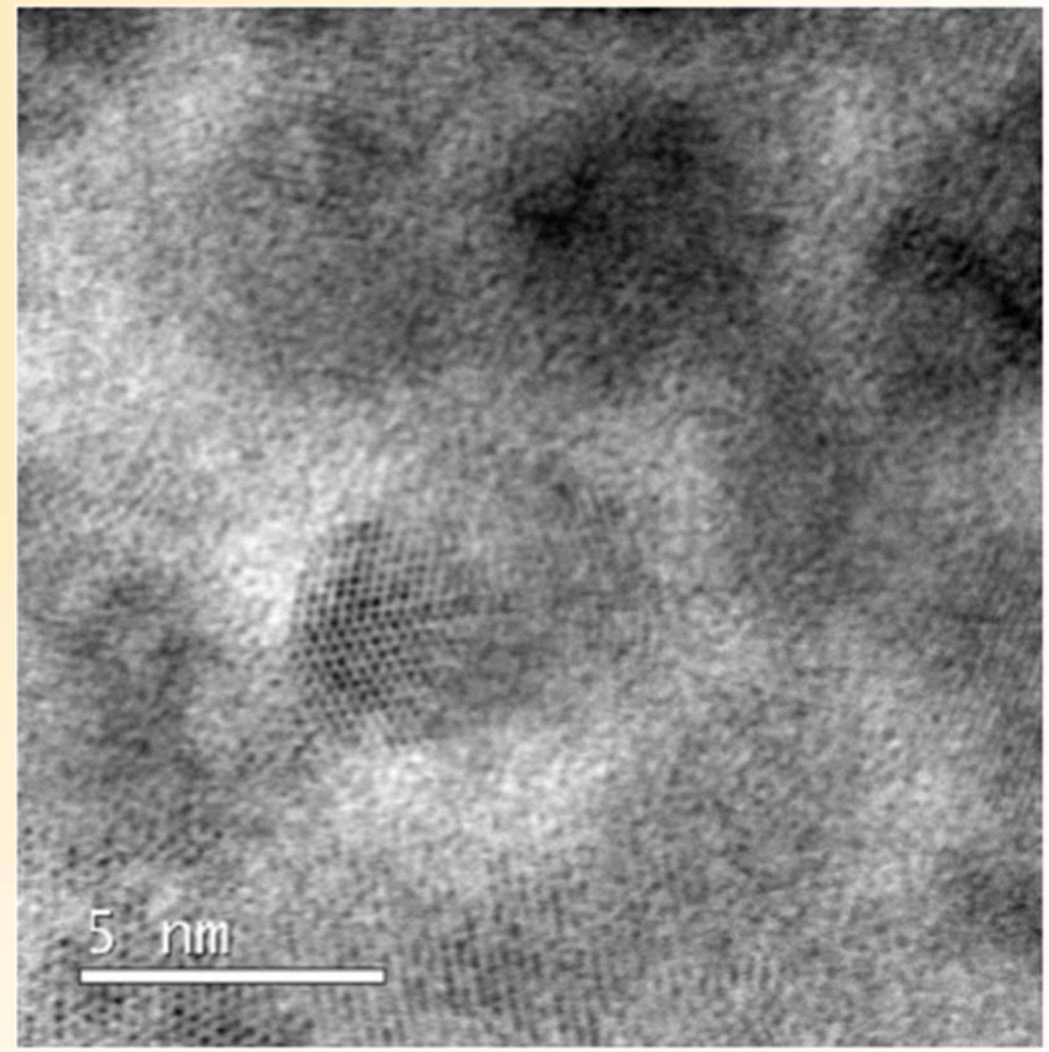

High magnification STEM image, revealing presence of in-grain metastable and crystalline precipitate phase (~ 5nm)

High Amounts of Grain Boundary Impurities

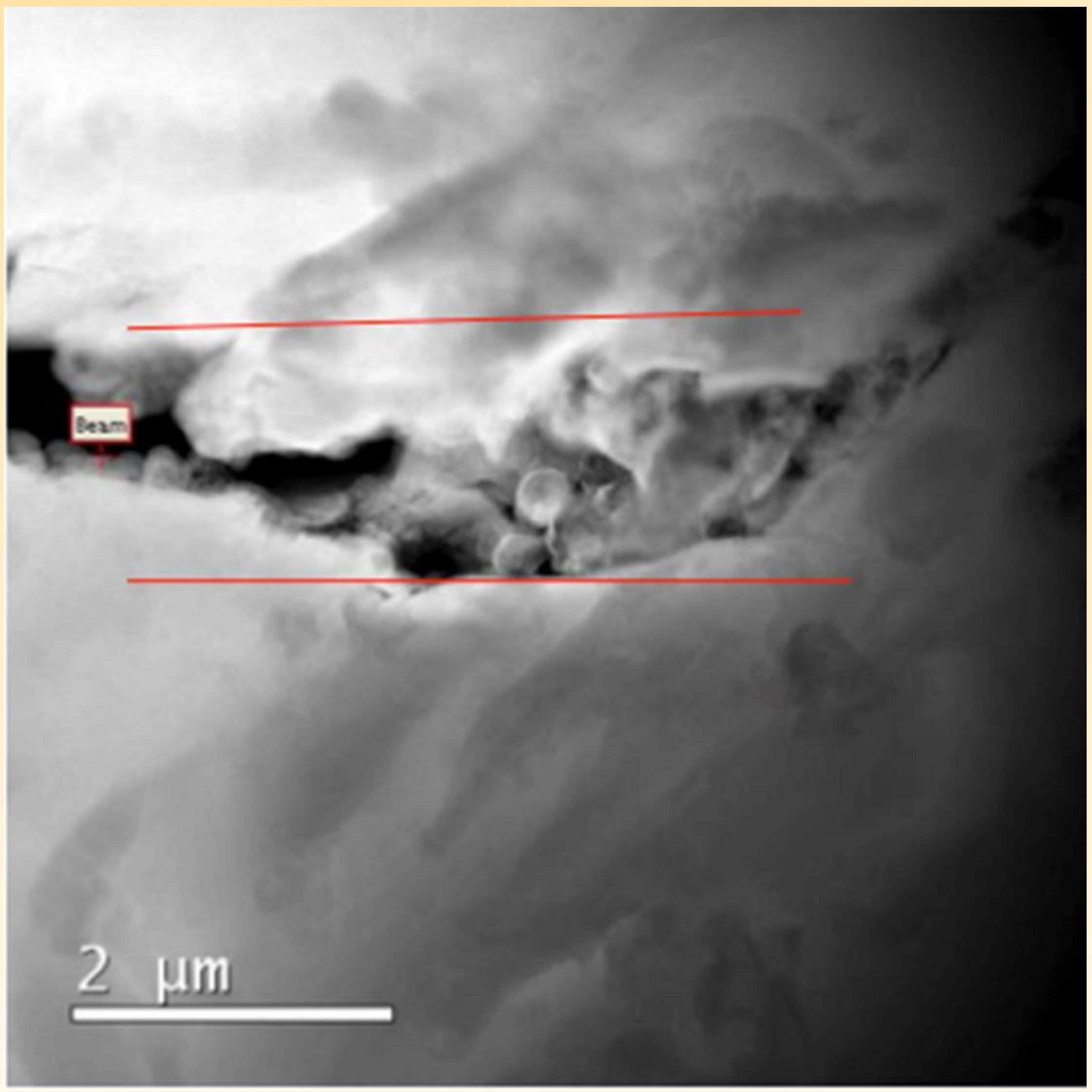

STEM image of grain boundary region containing many grain-boundary phases/impurities (~0.5 μm)

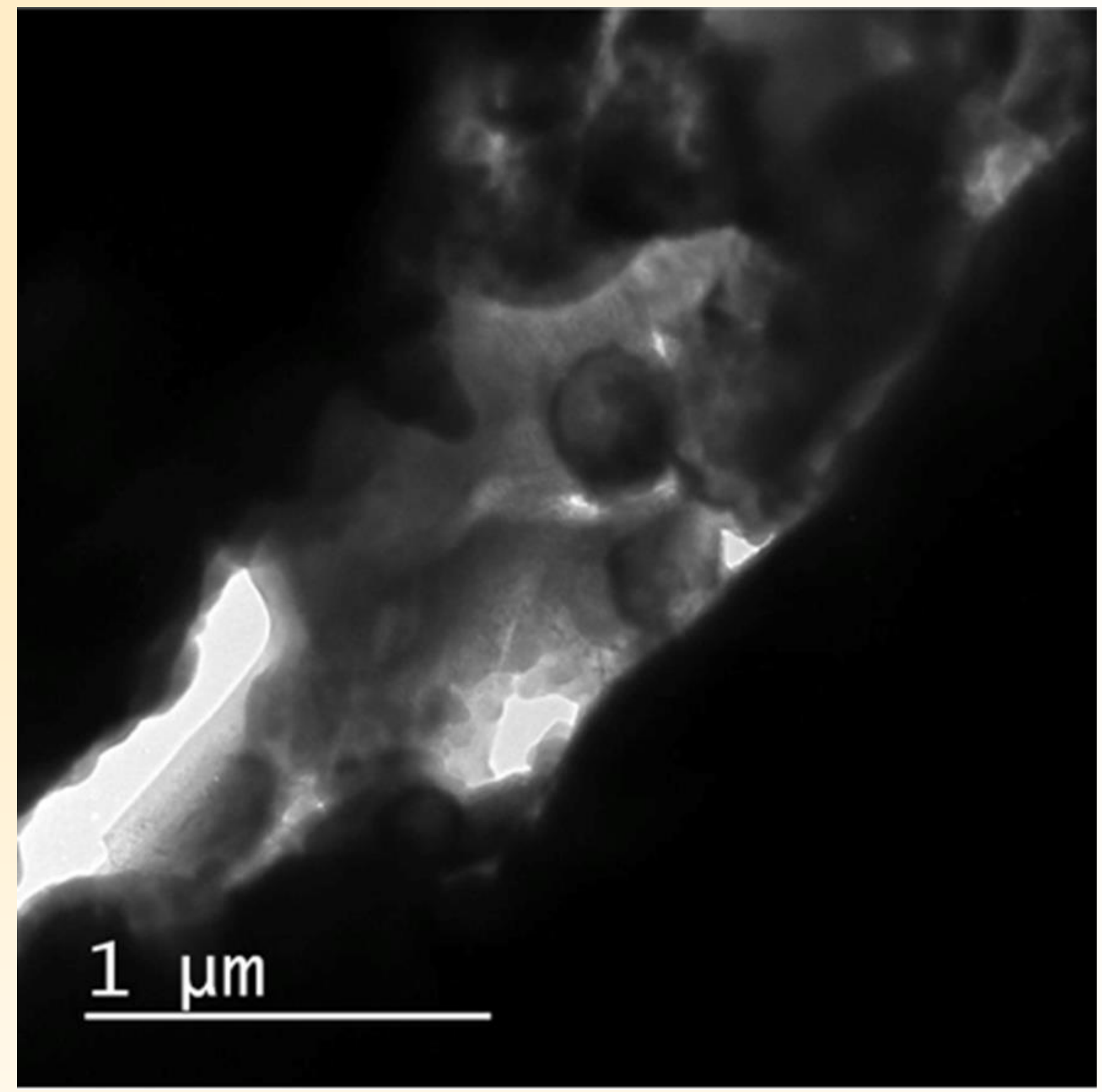

Higher magnification TEM image revealing phases along grain boundary impurity particles

Dark Field Contrast Imaging of γ''Precipitates

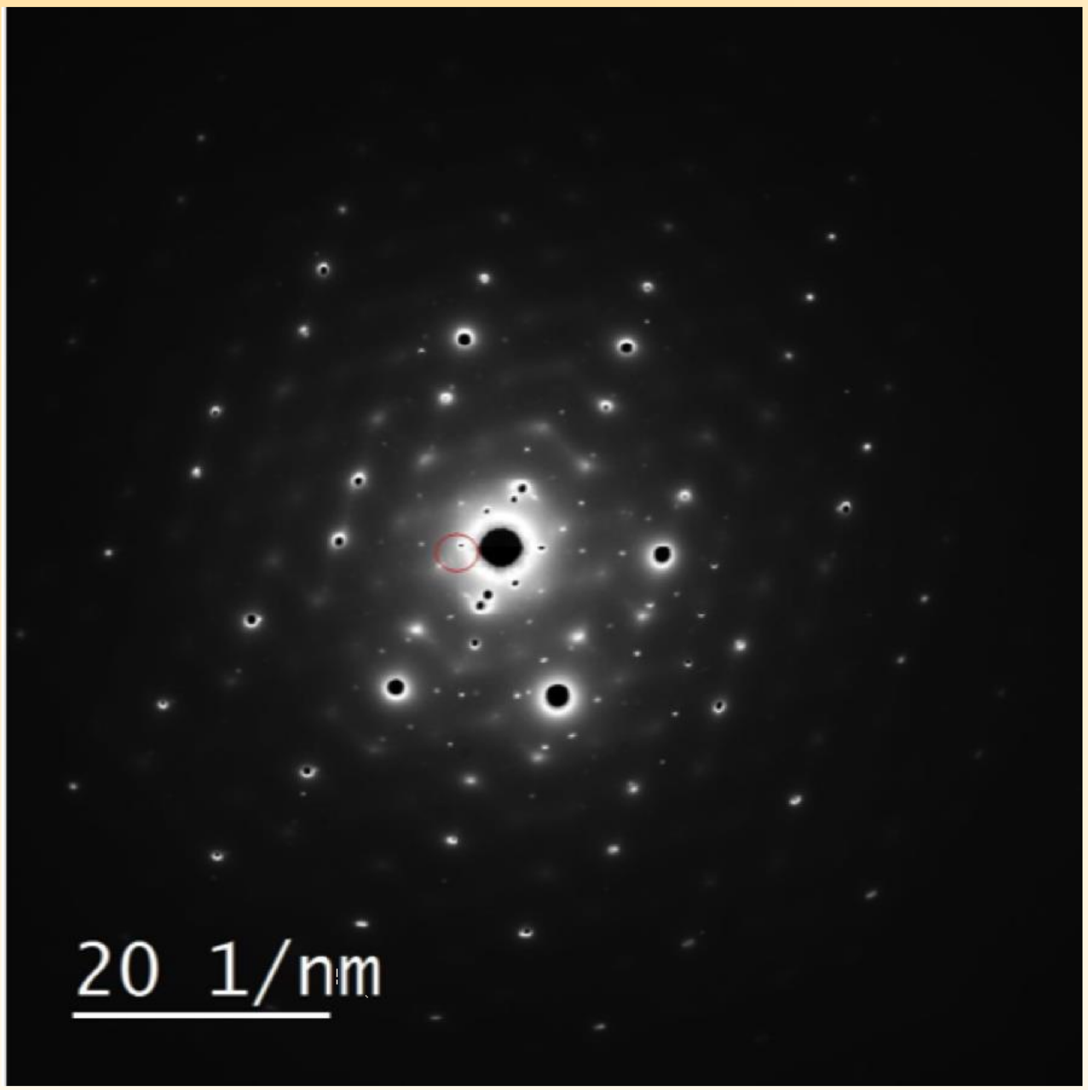

SAD used to create DF image on the right, the intensity and number of impurity Bragg reflections indicate a fairly large impurity particle concentration, and the red circle indicates the spot used to create the dark field image

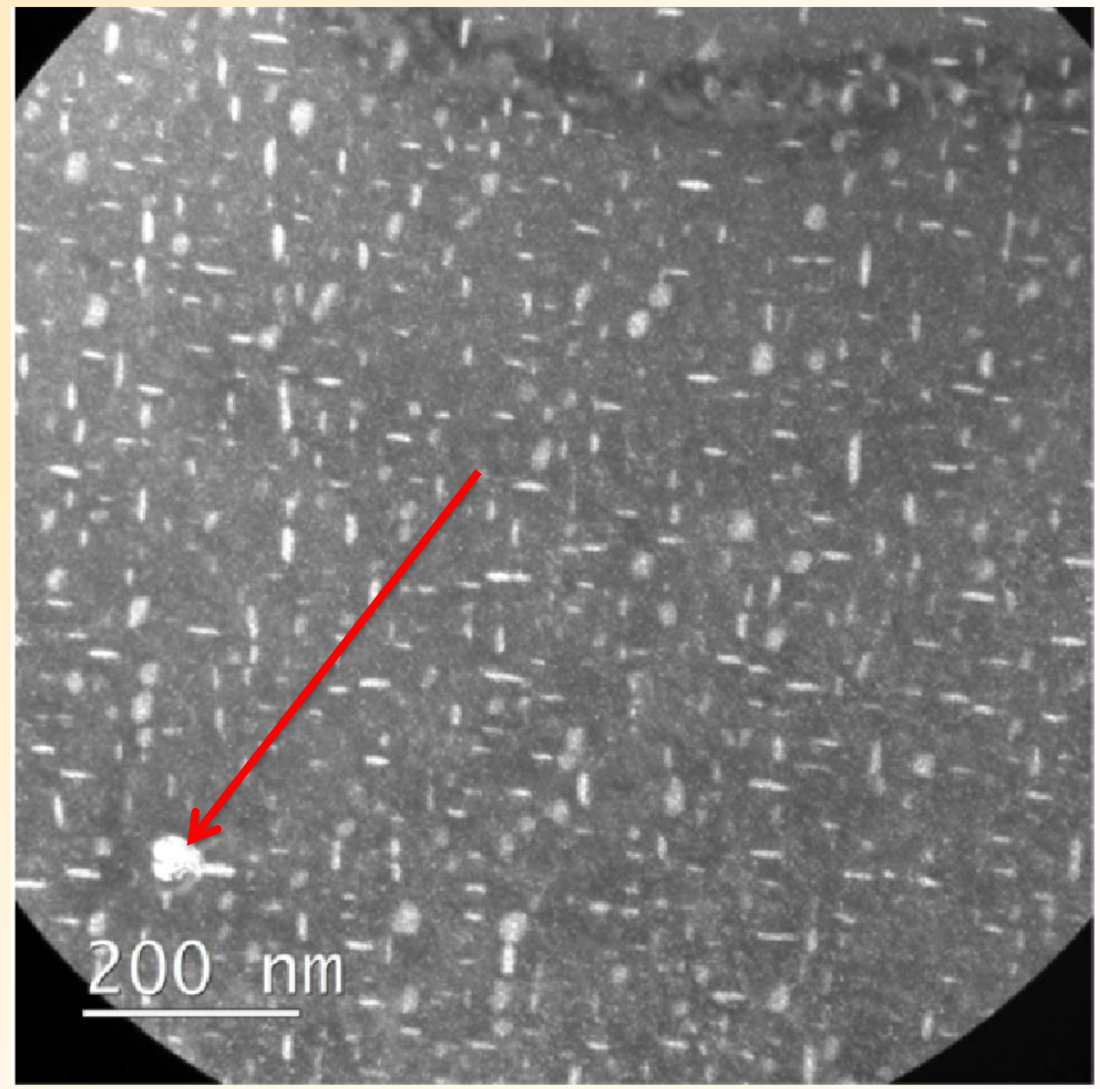

Dark field image showing high-density small intermetallic precipitates with morphology similar to that reported in literature

Twin Boundaries and Impurity Distributions

- Twin boundary showing high dislocation density
- Twin boundaries don’t appear to be decorated with impurity particles

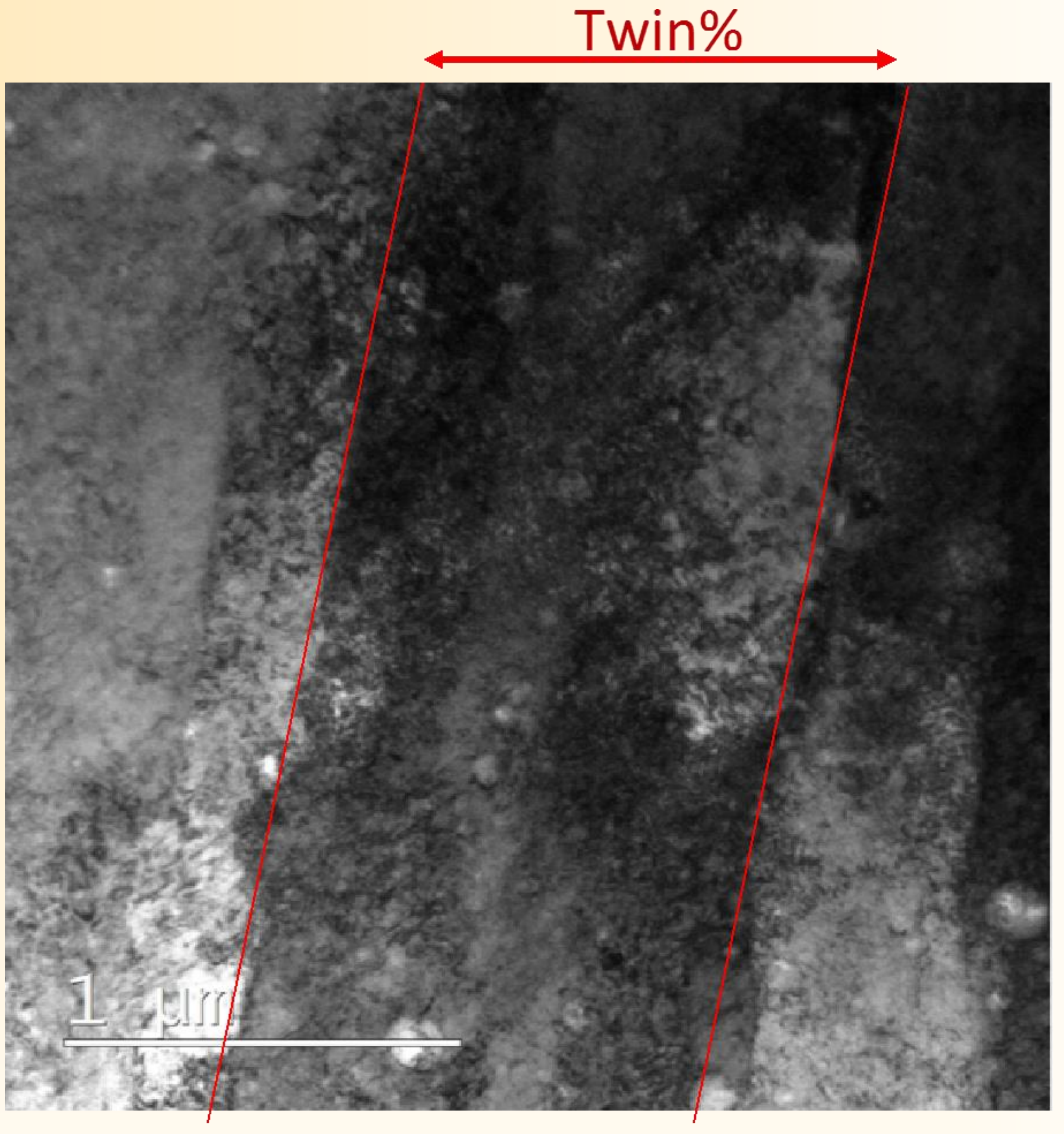

Lower Concentrations of Impurities found in Conventional Samples

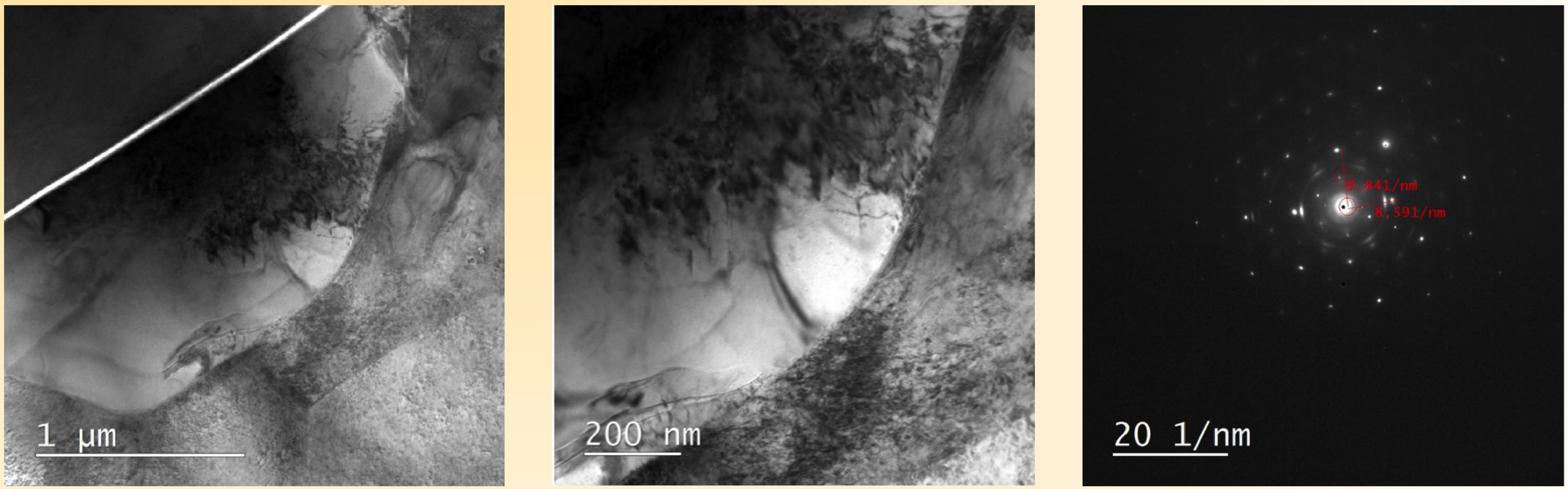

TEM images of conventionally wrought IN718 show fewer impurity phases than did DMLS prepared samples, further diffraction analysis confirms this, the diffraction pattern used for analysis is shown in the figure on the far right.

Thermal Modeling of DMLS Process

Goals

- Produce code that would predict heating and cooling events
- Accomplish 1D case
- Compare results to literature

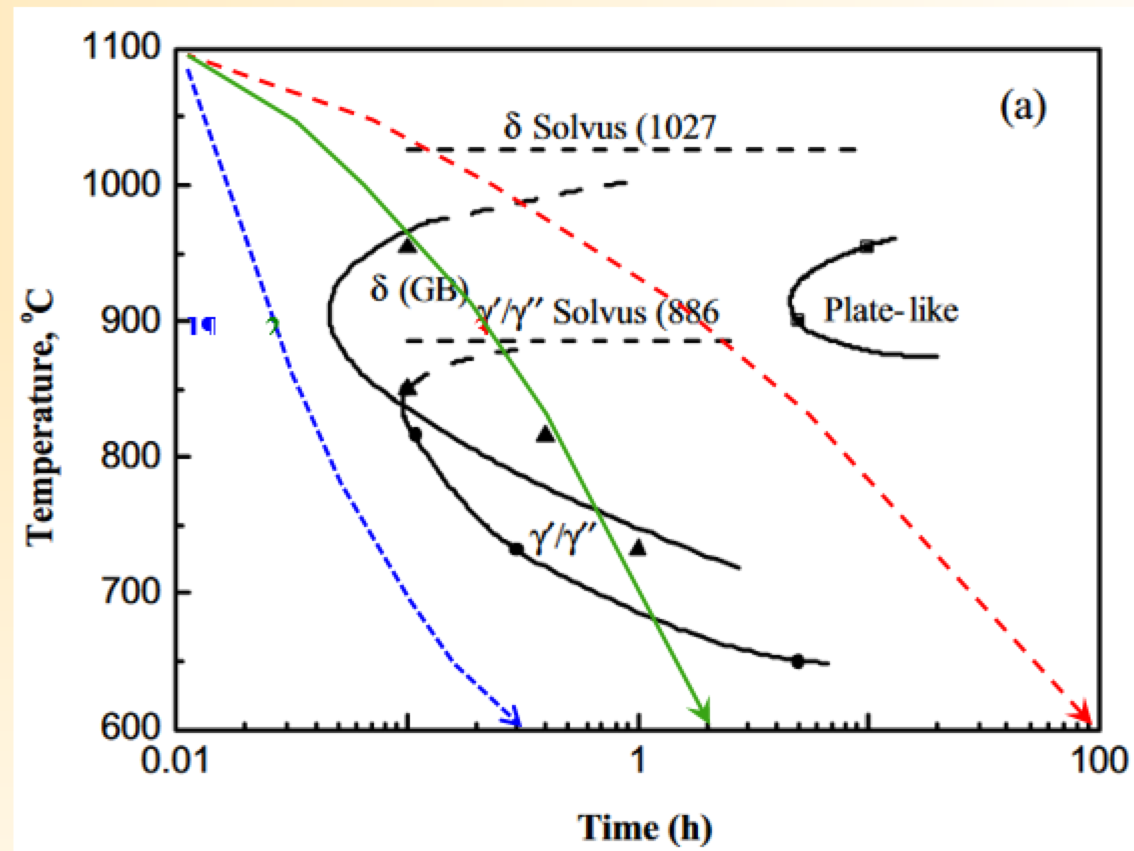

Comparison of Results and Literature Figure

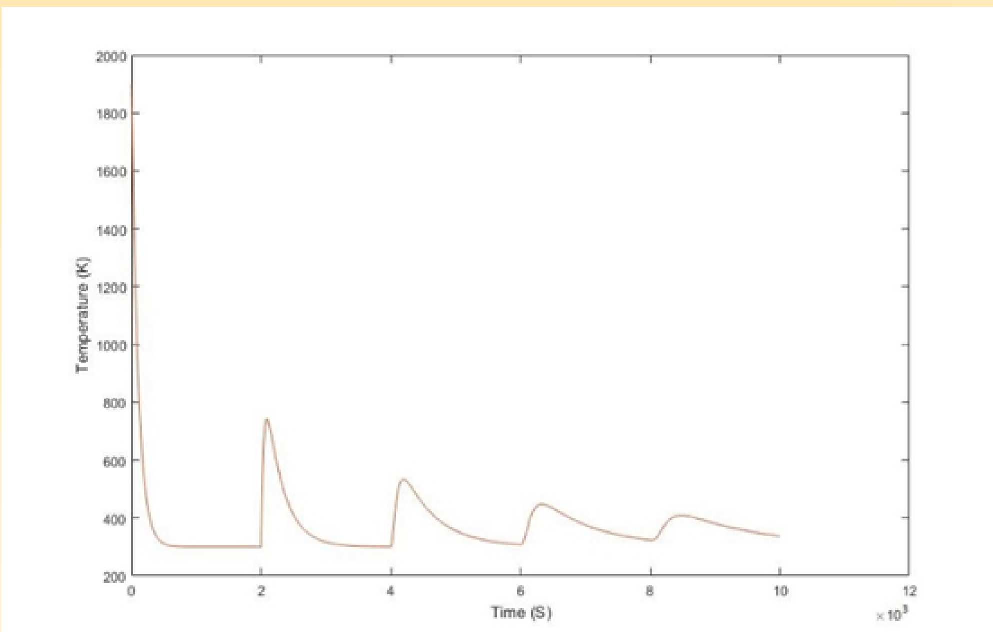

. Computed historical Temperature for layer 1 in a 5-layer system

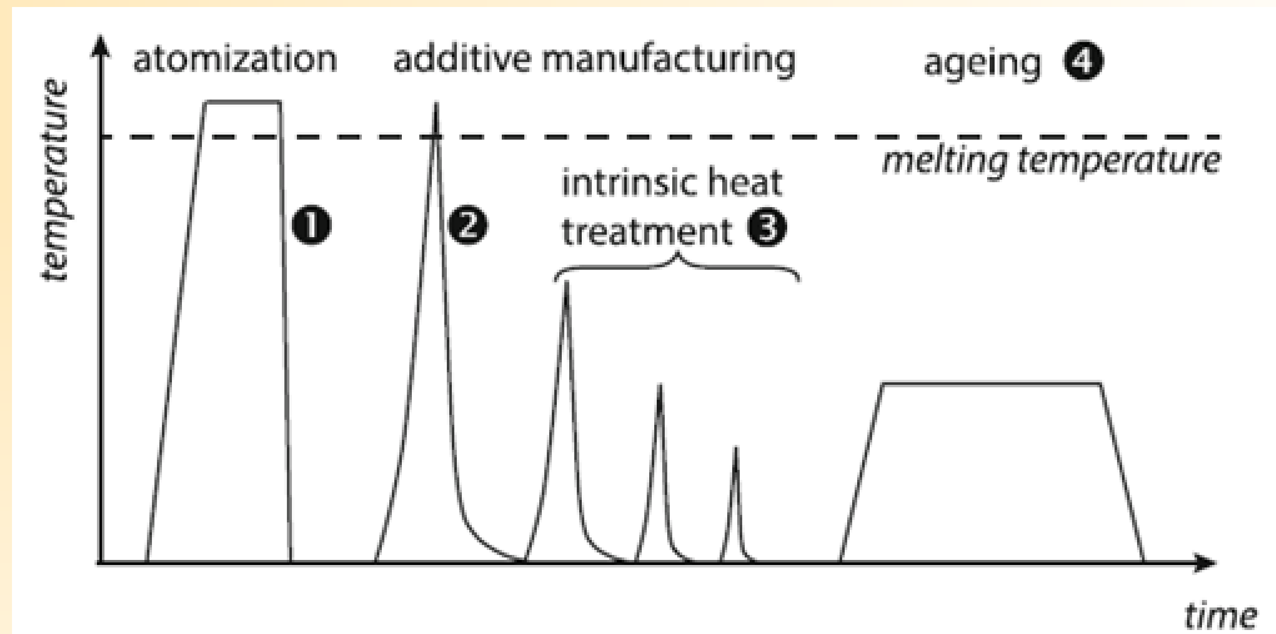

. Schematic image of the complex temperature–time profile experienced in the course of the production of an additively manufactured part. The numbers designate specific processing steps when precipitation, desired and undesired, may occur
Source:
Jägle, Eric A. et al. "Precipitation Reactions in Age-Hardenable Alloys During Laser Additive Manufacturing." *Jom*, vol. 68, no. 3, 2016, pp. 943-949, doi:10.1007/s11837-015-1764-2.

Implications of Results

- Ability to tailor materials properties using strategic rastering appears to be possible

- Thermal history can be predicted with fairly simple calculation

- Expansion of model to 3D could provide rout to optimization capability and provide new level of material property control

Summary

A literature review of DMLS processing and IN718 indicates presence of stress induced microstructural developments

Creep rupture data indicates a change in creep mechanism for wrought IN718 that is not present in DMLS IN718, and shows superior creep resistance in DMLS samples

SEM and TEM studies confirm presence of high dislocation density, high energy grain boundaries, and reveal a higher concentration of impurity phases in DMSL processed IN718 than in wrought IN718

Thermal modeling successfully identifies complex microstructural development of DMLS processed materials and shows promise for automated optimization of process